


## Article

# Design, Synthesis, In Vitro Biological Activity Evaluation and Stabilized Nanostructured Lipid Carrier Formulation of Newly Synthesized Schiff Bases-Based TMP Moieties

Syed Nasir Abbas Bukhari <sup>1,\*</sup>, Mohamed Y. Zakaria <sup>2</sup>, Muhammad Usman Munir <sup>1</sup>, Naveed Ahmad <sup>3</sup>, Mervat A Elsherif <sup>4</sup>, Rasha Emad Badr <sup>5</sup>, Ahmad Khalaf Hassan <sup>6</sup>, Ali H. Abu Almaaty <sup>6</sup> and Islam Zaki <sup>7,\*</sup>

- <sup>1</sup> Department of Pharmaceutical Chemistry, College of Pharmacy, Jouf University, Sakaka 72388, Saudi Arabia; mumunir@ju.edu.sa
  - <sup>2</sup> Department of Pharmaceutics and Industrial Pharmacy, Faculty of Pharmacy, Port Said University, Port Said 42526, Egypt; dr\_m\_yehia@live.com
  - <sup>3</sup> Department of Pharmaceutics, College of Pharmacy, Jouf University, Sakaka 72388, Saudi Arabia; nakahmad@ju.edu.sa
  - <sup>4</sup> Chemistry Department, College of Science, Jouf University, Sakaka 72388, Saudi Arabia; maelsherif@ju.edu.sa
  - <sup>5</sup> Clinical and Chemical Pathology Department, Faculty of Medicine, Port Said University, Port Said 42526, Egypt; dr.rashaemad@hotmail.com
  - <sup>6</sup> Zoology Department, Faculty of Science, Port Said University, Port Said 42526, Egypt; ahkhalaf71@yahoo.com (A.K.H.); ali\_zoology\_2010@yahoo.com (A.H.A.A.)
  - <sup>7</sup> Pharmaceutical Organic Chemistry Department, Faculty of Pharmacy, Port Said University, Port Said 42526, Egypt
- \* Correspondence: sbukhari@ju.edu.sa (S.N.A.B.); eslam.zaki@pharm.psu.edu.eg (I.Z.); Tel.: +966-565738896 (S.N.A.B.); +201-153436140 (I.Z.)



**Citation:** Bukhari, S.N.A.;

Zakaria, M.Y.; Munir, M.U.;

Ahmad, N.; Elsherif, M.A.; Badr, R.E.;

Hassan, A.K.; Almaaty, A.H.A.;

Zaki, I. Design, Synthesis, In Vitro

Biological Activity Evaluation and

Stabilized Nanostructured Lipid

Carrier Formulation of Newly

Synthesized Schiff Bases-Based TMP

Moieties. *Pharmaceuticals* **2022**, *15*,

679. [https://doi.org/10.3390/](https://doi.org/10.3390/ph15060679)

ph15060679

Academic Editor: Mary J. Meegan

Received: 27 April 2022

Accepted: 26 May 2022

Published: 28 May 2022

**Publisher's Note:** MDPI stays neutral with regard to jurisdictional claims in published maps and institutional affiliations.



**Copyright:** © 2022 by the authors. Licensee MDPI, Basel, Switzerland. This article is an open access article distributed under the terms and conditions of the Creative Commons Attribution (CC BY) license (<https://creativecommons.org/licenses/by/4.0/>).

**Abstract:** A series of novel Schiff bases-based TMP moieties have been designed and synthesized as potential anticancer agents. The target Schiff bases were screened for their cytotoxic activity against the MDA-MB-231 breast cancer cell line. Most of the tested molecules revealed good cytotoxic activity, especially compounds **4h**, **4j** and **5d**. Being the most potent, compound **4h** showed good tubulin polymerization inhibition activity as revealed by immunofluorescence analysis and ELISA assay. Additionally, compound **4h** was screened for cell cycle disturbance and apoptosis induction. Pre-G1 apoptosis and cell growth halt at the G2/M phase were discovered to be caused by it. Moreover, compound **4h** induced apoptosis via p53 and Bax activation, as well as reduced the level of Bcl-2. Additionally, the most potent compound **4h** was lodged on nanostructured lipid carriers (NLCs). <sup>23</sup> full factorial design was involved to govern the influence of the fabrication variables on the in vitro characters of the casted NLCs. F3 was picked as the optimum formula exhibiting dominant desirability value 0.805, EE% 95.6 ± 2.4, PS 222.4 ± 18.7, PDI 0.23 ± 0.05 and ZP -39.2 ± 3.9 Mv. Furthermore, F3 affirmed improved solubility and release over the drug suspension. In the comparative cytotoxic activity, F3 was capable of diminishing the IC<sub>50</sub> by around 2.15 times for pure **4h**, while nearly close to the IC<sub>50</sub> of the reference drug. Thus, NLCs could be a potential platform for boosted antitumor activity.

**Keywords:** TMP; Schiff base; synthesis; cytotoxicity; tubulin; cell cycle analysis; annexin V; p53; Bax; Bcl-2

## 1. Introduction

Microtubules are among the most important molecular targets for cancer chemotherapeutic treatment [1–3]. The formation of microtubules is a dynamic process that involves the assembly and disassembly of  $\alpha$  and  $\beta$ -tubulin subunits [4–6]. A chemotherapeutic agent binds to tubulin and interferes with this dynamic stability, and thus

induces cell cycle disturbance, resulting in apoptosis induction and cell death [7–9]. Compounds containing trimethoxyphenyl (TMP) ring have been reported to have excellent potent cytotoxic activity against a broad range of cancer cell lines through inhibition of  $\alpha$  and  $\beta$ -tubulin dynamic equilibrium [10–13]. The creation of tubulin polymerization inhibitors has been the subject of several investigations in recent years. As a result, anticancer medicines with tubulin polymerization inhibitory activity have been designed and developed using TMP-containing compounds. [14–16]. Colchicine (Col) **I**, combretastatin A-4 (CA-4) **II** and phenstatin **III** are natural compounds that bind to the colchicine binding site and prevent the polymerization of tubulins to form microtubules [17–19]. In addition, PIB-SA **IV** efficiently inhibited tumor proliferation similar to that of CA-4 [20]. Moreover, compound **V** showed strong antiproliferative activity against four human cancer cell lines with  $IC_{50}$  values of 3–9 nM, as well as high selectivity to normal cells [21]. Additionally, the *bis*-hydrazide molecule **VI** displayed 83.1% in vitro tubulin polymerization inhibition activity at its  $IC_{50}$  dose level [22] (Figure 1).

A literature survey revealed that Schiff base derivatives are known for their various biological activities [23–25]. In addition, many Schiff bases exhibited promising antitumor potency against different cancer cell lines [26–28]. The Schiff base possessing TMP ring **VII** showed antiproliferative activity against the MCF-7 breast cancer cell line with an  $IC_{50}$  value of 0.87  $\mu$ M [26]. Furthermore, Schiff base **VIII** possessing *N*-furylmethylidene moiety was identified as a potent antiproliferative agent against many cancer cell lines [28].

On the basis of the aforementioned structural analysis, as well as in keeping with our general enthusiasm for the design and development of novel anticancer agents, [29–32], as potential anticancer medicines, the current work focused on the design and synthesis of novel Schiff bases-based TMP moieties. The basic structural skeleton of the lead compound is formed from two TMP rings connected through amide-acrylic acid hydrazide groups. The target molecules were intended to have different aliphatic and aromatic side chains at the hydrazide group to study the impact of these structural variations on antiproliferative activity. The hydrazide group in the lead compound was subjected to the replacement of the amino ( $NH_2$ ) group to give *N*-ethylidene hydrazinyl derivative **2**. In addition, further structure extension of hydrazide group with furan or substituted phenyl moieties afforded *N*-furylmethylidene hydrazinyl derivative **3** or *N*-arylidene hydrazinyl molecules **4a–5g**, respectively (Figure 2). The MDA-MB-231 cell line was used to test the cytotoxic activity of the target compounds. Additional studies were conducted on the most potent compound, **4h**, including DNA flow cytometry and tubulin polymerization inhibition, as well as apoptotic-related tests. In addition, the most potent and promising drug was incorporated in nanostructured lipid carriers (NLCs) as an attempt to improve its solubility and other kinetic parameters, thereby boosting its cytotoxicity. This was attained by the formulation of 8 NLCs formulae of different compositions obtained from  $2^3$  full factorial design and the impact of the formulation variables on the EE%, PS and ZP was analyzed by Stat-Ease® V.13 software (Design-Expert TM; Minneapolis, MN, USA). Then, the optimum formula was selected and involved in further characterization especially the comparative cytotoxicity study relative to the pure drug to demonstrate the influence of the NLCs of  $IC_{50}$  on the compound.

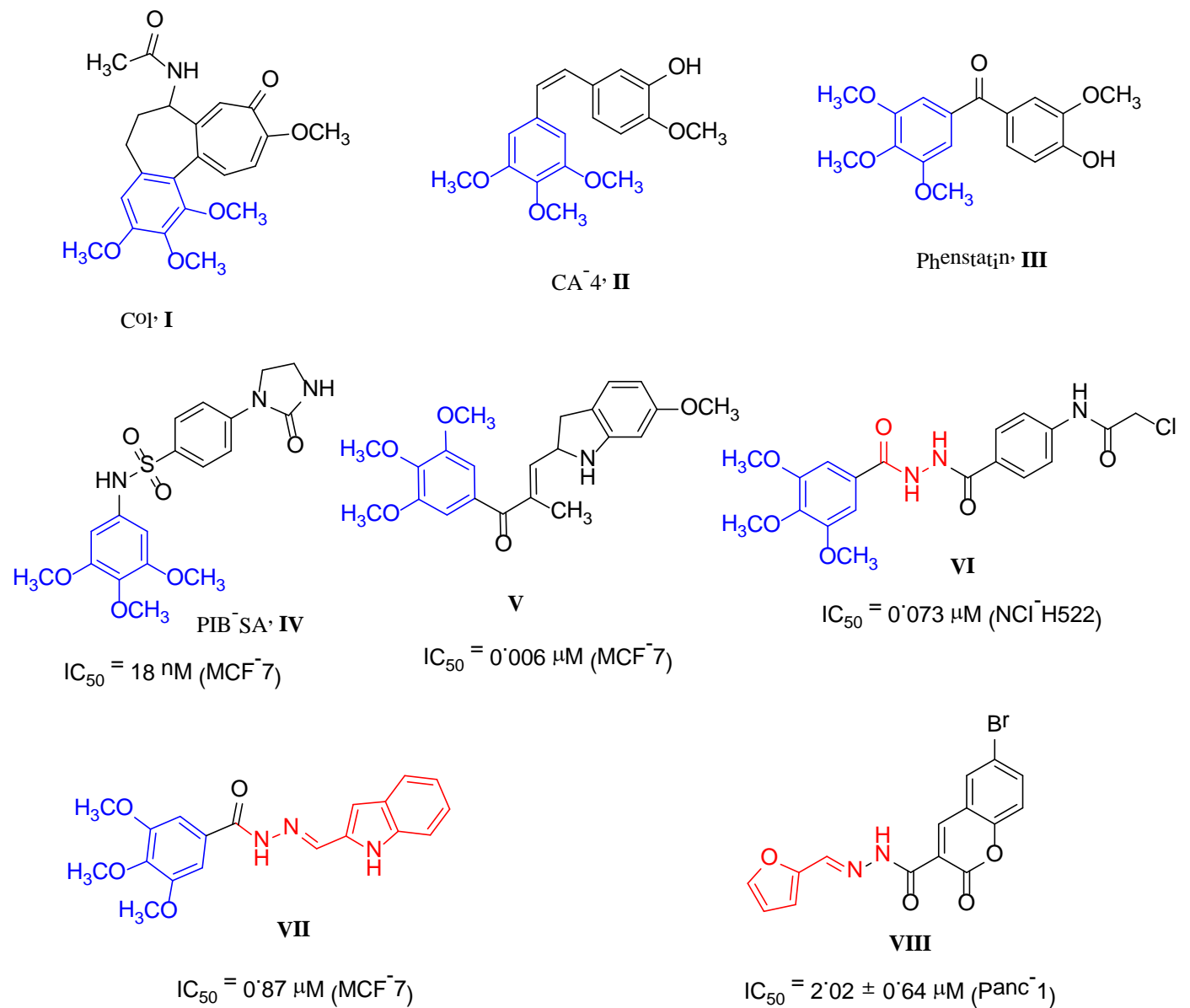


**Figure 1.** Chemical structure of reported tubulin polymerization inhibitors containing TMP moiety (I–VI) and reported Schiff base derivatives (VII–VIII) possessing anticancer activity.

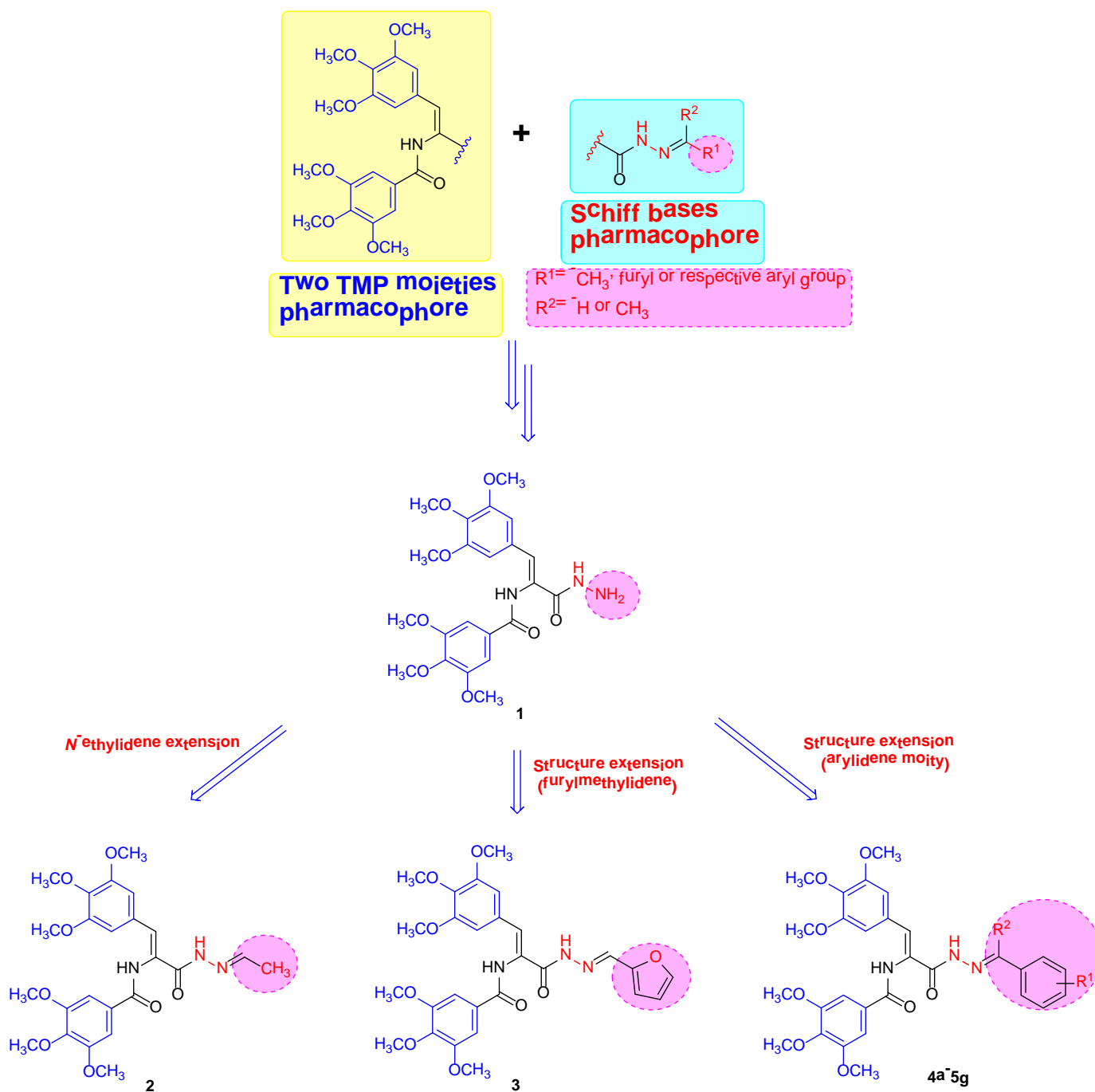


Figure 2. Design strategy of the prepared compounds 2–5g.

## 2. Results and Discussion

### 2.1. Chemistry

The synthesis of target Schiff bases-based TMP compounds is outlined in Scheme 1. The reaction of hydrazide 1 with acetaldehyde, furfural or different aromatic aldehyde in absolute ethanol in the presence of catalytic amounts of glacial acetic acid produced the corresponding *N*-(3-((*Z*)-2-Ethylidenehydrazinyl)-3-oxo-1-(3,4,5-trimethoxyphenyl)prop-1-en-2-yl)-3,4,5-trimethoxybenzamide (2), *N*-(3-((*E*)-2-(Furan-2-ylmethylene)hydrazinyl)-3-oxo-1-(3,4,5-trimethoxyphenyl)prop-1-en-2-yl)-3,4,5-trimethoxybenzamide (3) or *N*-(3-((*E*)-2-(Aryl)hydrazinyl)-3-oxo-1-(3,4,5-trimethoxyphenyl)prop-1-en-2-yl)-3,4,5-trimethoxybenzamides 4a–I, respectively. In the same manner, condensing the hydrazide 1 with convenient aryl ketone in *n*-butanol furnished the corresponding *N*-(3-

((*E*)-2-(Arylethylidene)hydrazinyl)-3-oxo-1-(3,4,5-trimethoxyphenyl)prop-1-en-2-yl)-3,4,5-trimethoxybenzamides **5a–g**, respectively. The structure of the prepared Schiff bases was confirmed by elemental analysis and spectral data ( $^1\text{H-NMR}$  and  $^{13}\text{C-NMR}$  spectra) and were consistent with the proposed structures.  $^1\text{H-NMR}$  spectra of compound **2** showed the presence of four proton peaks; at  $\delta$  10.00 and 9.89 ppm attributed to two amidic (NH) protons, at  $\delta$  9.85 ppm due to proton attached to imine carbon and at  $\delta$  1.89 ppm related to methyl protons attached to imine carbon ( $\text{CH}_3\text{C}=\text{N}$ ).  $^{13}\text{C-NMR}$  spectra of **2** showed the presence of two characteristic carbon signals; at  $\delta$  164.60 ppm corresponding to (C=N) carbon and at  $\delta$  21.08 ppm related to methyl carbon ( $\text{CH}_3\text{C}=\text{N}$ ). In addition,  $^1\text{H-NMR}$  spectra of compounds **3** and **4a–l** showed three singlet signals at  $\delta$  11.32–12.02 and 10.00–10.10 ppm related to two amidic (NH) protons and at  $\delta$  8.29–8.85 ppm corresponding to characteristic azomethine (N=CH) proton. In addition,  $^1\text{H-NMR}$  spectra of compounds **3** and **4a–l** showed additional signals at the aromatic region corresponding to the presence of furan or substituted phenyl moiety.  $^{13}\text{C-NMR}$  spectra of compounds **3** and **4a–l** showed a characteristic signal at  $\delta$  144.84–148.83 ppm related to azomethine (N=CH) carbon and two signals at  $\delta$  165.66–165.75 and 162.02–163.18 ppm related to two amide groups. Additionally, the formation of Schiff bases **5a–g** was confirmed by  $^1\text{H-NMR}$  and  $^{13}\text{C-NMR}$  spectral studies.  $^1\text{H-NMR}$  revealed the presence of three peaks at  $\delta$  10.43–10.63 and 10.05–10.10 ppm corresponding to two amidic (NH) protons and at  $\delta$  2.23–2.31 ppm related to methyl group attached to imine carbon.  $^{13}\text{C-NMR}$  spectra of **5a–g** confirmed the carbon skeleton due to the presence of two signals at  $\delta$  145.73–149.84 ppm related to imine (C=N) carbon and at  $\delta$  14.82–15.33 ppm corresponds to the methyl group attached to imine carbon ( $\text{CH}_3\text{C}=\text{N}$ ). Furthermore,  $^{13}\text{C-NMR}$  of **5a–g** revealed a set of signals that appeared in the aromatic region related to aromatic carbons.

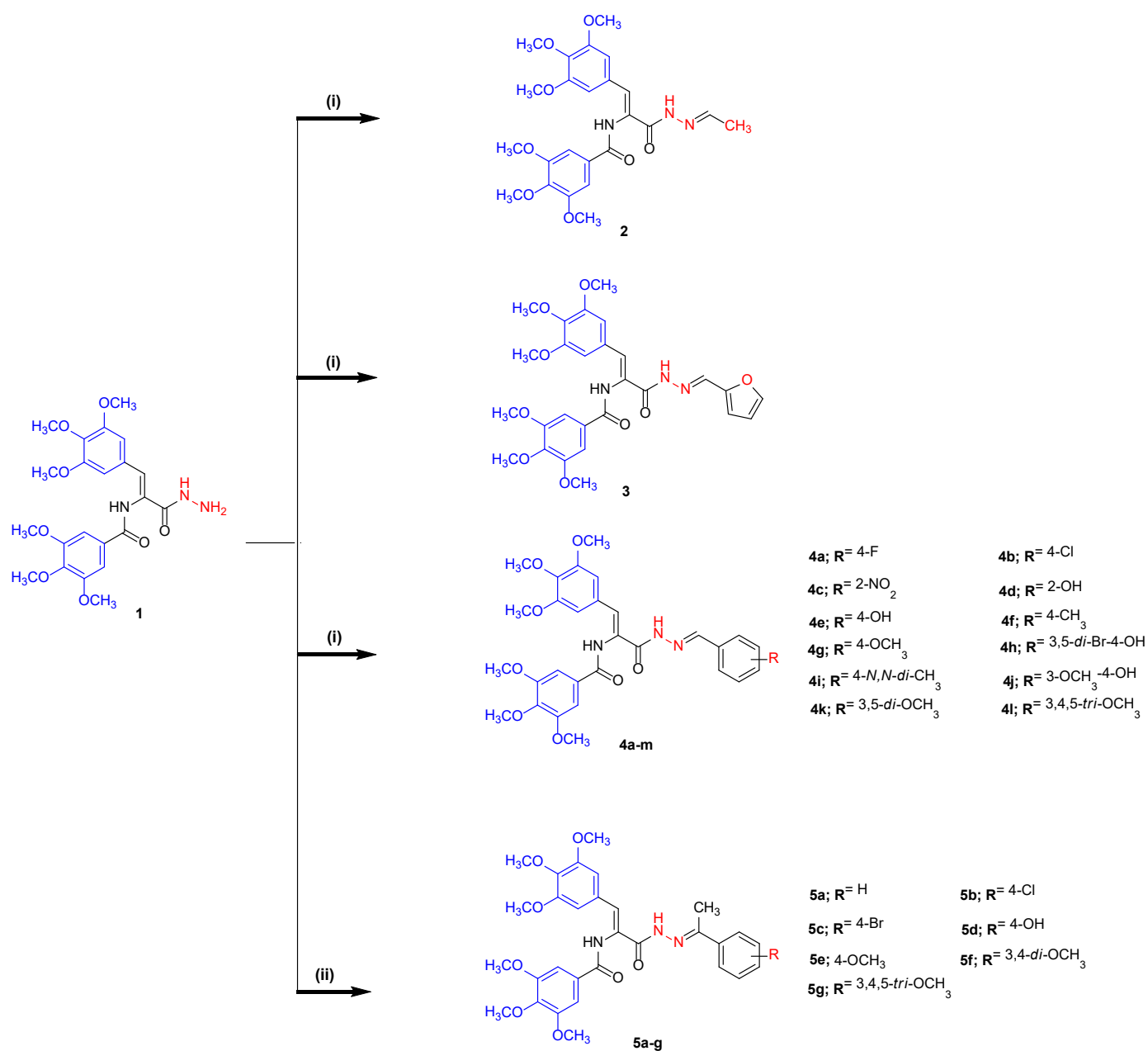
## 2.2. Biology

### 2.2.1. Cytotoxic Assay against MDA-MB-231 Breast Cancer Cell Line

The newly prepared Schiff bases **2–5g** were screened for their *in vitro* cytotoxic activity against the MDA-MB-231 breast cancer cell line taking CA-4 as a reference drug. From the obtained results presented in Table 1, it is obvious that *N*-ethylidene hydrazinyl derivative **2** revealed weak cytotoxic activity ( $\text{IC}_{50} = 31.59 \pm 1.07 \mu\text{M}$ ). Replacement of methyl group in compound **2** by furan ring produced a compound with improved cytotoxic activity ( $\text{IC}_{50} = 6.08 \pm 0.42 \mu\text{M}$ ). In addition, further structure extension to give *N*-aryl hydrazinyl molecules **4a–5g** produced compounds with considerable cytotoxic activity, which may give an indication that the aryl ring is important for cytotoxic activity. Compounds **4h**, **4j** and **5d** ( $\text{IC}_{50} = 2.84 - 1.27 \mu\text{M}$ ) are the most potent in this study and possess cytotoxic activity comparable to reference compound CA-4 ( $\text{IC}_{50} = 0.54 \pm 0.04 \mu\text{M}$ ). Furthermore, the 3,5-dibromo-4-hydroxybenzylidene hydrazinyl derivative **4h** has proven to be the most potent cytotoxic compound with  $\text{IC}_{50} = 1.27 \pm 0.18 \mu\text{M}$ . Additionally, the most potent cytotoxic compound showed a higher  $\text{IC}_{50}$  value ( $\text{IC}_{50} = 30.83 \pm 2.32 \mu\text{M}$ ) against normal breast cell line MCF-10A; therefore, Schiff base **4h** can be considered to be selective molecules with a safe mode of action toward normal breast cell lines.

### 2.2.2. Tubulin Polymerization Inhibition Assays

Several investigations have shown that TMP-containing compounds such as Col and CA-4 interact with tubulin at the colchicine binding site, inhibiting microtubule assembly [33]. The effects of representative Schiff bases on the inhibition of tubulin assembly were evaluated. Compound **4h** which demonstrated potent cytotoxic activity was assessed at its  $\text{IC}_{50}$  concentration. Tubulin polymerization inhibitory activity against the MDA-MB-231 cell line was investigated by immunofluorescence analysis using a confocal microscope. The results demonstrated that compound **4h** exhibited good tubulin polymerization inhibition activity compared with the untreated cells (Figure 3A).



**Scheme 1.** Synthesis of the target compounds 2–5g. Reagent and reaction condition: (i) acetaldehyde, furfural or respective aryl aldehyde, EtOH, AcOH, reflux 6–8 h; (ii) respective aryl ketone, n-butanol, reflux 6–8 h.

**Table 1.** Cytotoxic screening of the tested Schiff bases 2–5g. Values are the mean of three independent replicates ± SE.

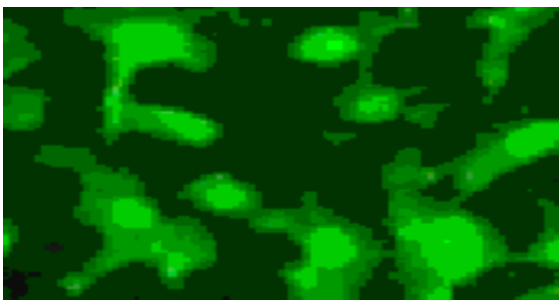
Compound No.	IC <sub>50</sub> Value (μM)	
	MDA-MB-231	MCF-10A
2	31.59 ± 1.07	NT
3	6.08 ± 0.42	NT
4a	23.70 ± 1.13	NT
4b	16.10 ± 0.83	NT
4c	38.82 ± 0.93	NT
4d	5.98 ± 0.28	NT

Table 1. Cont.

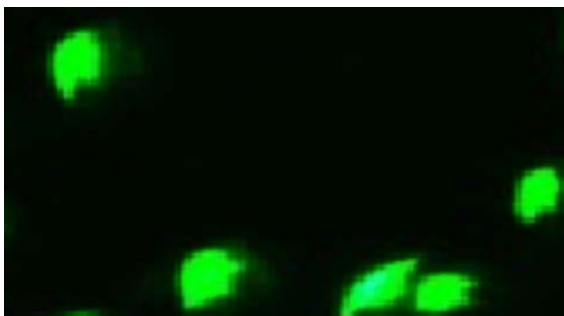
Compound No.	IC <sub>50</sub> Value (μM)	
	MDA-MB-231	MCF-10A
4e	7.10 ± 1.02	NT
4f	4.52 ± 0.36	NT
4g	3.43 ± 0.22	NT
4h	1.27 ± 0.18	30.83 ± 2.32
4i	3.46 ± 0.51	NT
4j	2.84 ± 0.18	NT
4k	4.80 ± 0.17	NT
4l	7.30 ± 0.64	NT
5a	20.15 ± 0.89	NT
5b	13.98 ± 1.19	NT
5c	20.73 ± 1.84	NT
5d	1.98 ± 0.19	NT
5e	9.52 ± 1.18	NT
5f	8.34 ± 1.22	NT
5g	3.39 ± 0.26	NT
CA-4	0.54 ± 0.04	8.86 ± 0.67

A)

CTRL MDA-MB-231



Comp 4h/ MDA-MB-231



B)

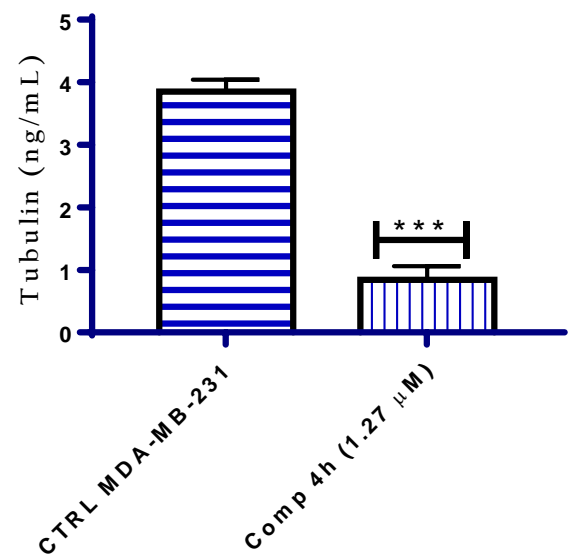


**Figure 3.** (A) Graphical representation of immunofluorescence analysis of tubulin localization in MDA-MB-231 cells after treatment with compound **4h** at its IC<sub>50</sub> concentration compared with no treatment control. (B) Graphical representation of tubulin concentration (ng/mL) before and after treatment with compound **4h**. All values are presented as mean value ± SD and statistical analyses were carried out using one-way analysis of variance (ANOVA) followed by Tukey's multiple comparison test (\*\*\*)  $p < 0.001$ .

In addition, compound **4h** was subjected to in vitro tubulin polymerization inhibitory activity assay using ELISA assay for  $\beta$ -tubulin. As anticipated, compound **4h** inhibited the polymerization of tubulin with a percent inhibition of 78.14% compared with no treatment control (Figure 3B). The results in this study suggested that the molecular target of the prepared Schiff base **4h** is indeed tubulin.

### 2.2.3. Cell Cycle Effects

For the purpose of studying the influence of these hydrazides on the cell cycle progression of MDA-MB-231 human malignant cell lines. A FACS analysis was used to determine the DNA proportion of cell nuclei. The treatment of MDA-MB-231 cells with compound **4h** at a concentration equal to its  $IC_{50}$  for 24 h induced apoptosis up to 31.27% of the pre-G1 phase and it was accompanied by a concomitant increase in the G2/M phase with a percentage value of 38.65% compared with value 8.22% of untreated control. Therefore, both increases in cells at pre-G1 and G2/M phases clearly show that Schiff base **4h** caused G2/M phase arrest and was effective in causing apoptosis in the case of MDA-MB-231 cancerous cells (Figure 4).

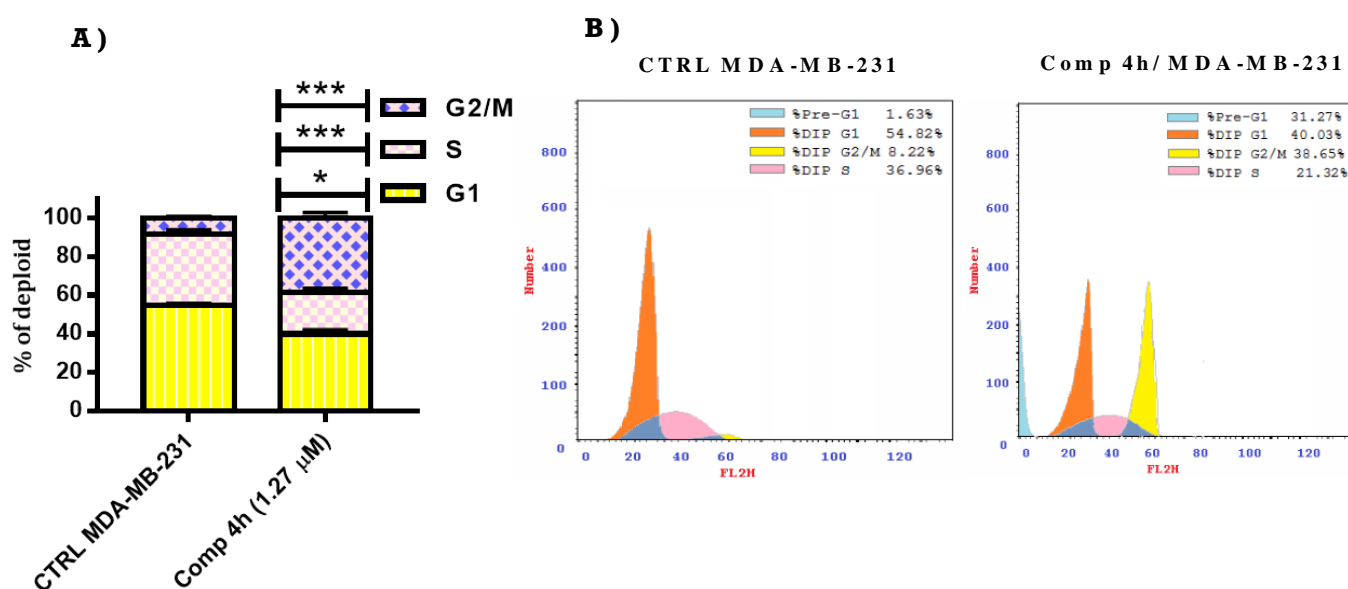


**Figure 4.** (A) Graphical representation for the effect of Schiff base **4h** on the cell cycle profile of MDA-MB-231 cells after 24 h. (B) Effect of Schiff base **4h** on the cell cycle profile of MDA-MB-231 cells after 24 h. All values are presented as mean value  $\pm$  SD and statistical analyses were carried out using one-way analysis of variance (ANOVA) followed by Tukey's multiple comparison test (\*  $p < 0.05$ , \*\*\*  $p < 0.001$ ).

### 2.2.4. Apoptosis Inducing Effect of Compound 4h

A double staining examination of annexin V FITC/propidium iodide (PI) was used to evaluate compound **4h**'s influence on apoptosis and estimate the percentage of the total, early, and late apoptosis in MDA-MB-231 cells. Compound **4h** treatment resulted in a higher proportion of overall apoptosis in the MDA-MB-231 cell line (31.27%) as compared to no treatment controls (1.63%). Furthermore, the proportion of early and late apoptotic cells rose by 23.12- and 63.67-fold, respectively, as compared to the untreated control cells. As supported by cell cycle effects and apoptosis assays of Schiff base **4h** revealed cell growth arrest at the G2/M phase as well as apoptosis-inducing activity (Figure 5).



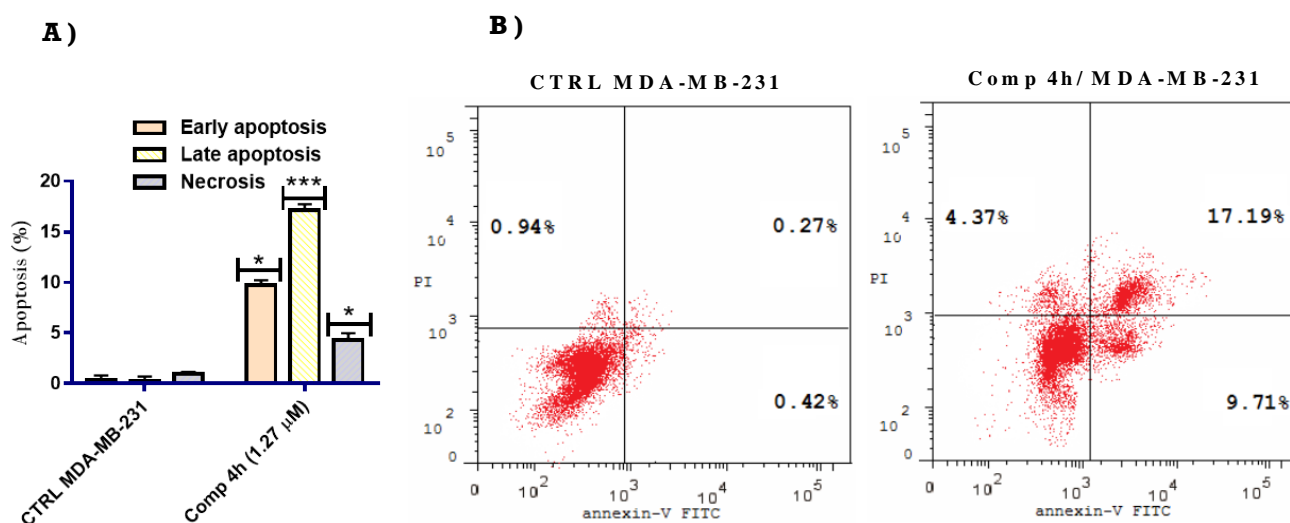


**Figure 5.** (A) Graphical representation for the effect of Schiff base **4h** on the induction of apoptosis in MDA-MB-231 cells after 24 h. (B) Effect of Schiff base **4h** on the induction of apoptosis in MDA-MB-231 cells after 24 h. All values are presented as mean value  $\pm$  SD and statistical analyses were carried out using one-way analysis of variance (ANOVA) followed by Tukey's multiple comparison test (\*  $p < 0.05$ , \*\*\*  $p < 0.001$ ).

#### 2.2.5. Mitochondrial Membrane Potential

Most of the known anticancer molecules induce apoptotic cascade via activation of the intrinsic pathway via release of cytochrome-c after depolarization of mitochondrial membrane [34]. The potential status of the mitochondrial membrane is determined by the electrochemical gradient ( $\Delta\psi$ ). In order to investigate the intrinsic pathway of apoptosis,  $\Delta\psi$  dissipation was measured by cytofluorometry by exposing the MDA-MB-231 cell line to compound for **4h** at a concentration equal to its  $IC_{50}$  for 24 h. The results in Figure 6 revealed a reduction in the level of MDA-MB-231  $MMP\psi$  by 65.23% in comparison with untreated cells as measured by flow cytometry. This indicates that compound **4h** induced mitochondrial dissipation in MDA-MB-231 cells, which in turn activated the intrinsic pathway of apoptosis and eventually triggered cell death via the apoptotic pathway.

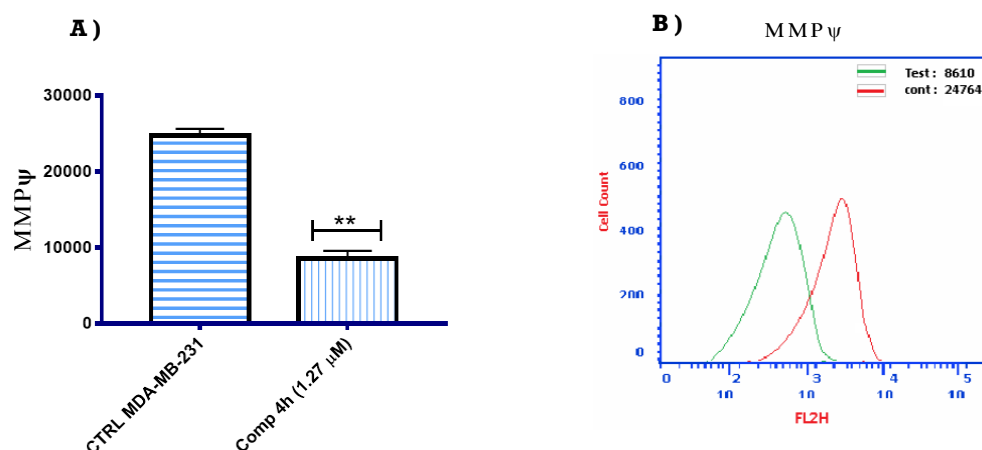


**Figure 6.** (A) Graphical representation for the effect of Schiff base **4h** on the mitochondrial membrane potential in MDA-MB-231 cells after 24 h. (B) Effect of Schiff base **4h** on the mitochondrial membrane potential in MDA-MB-231 cells after 24 h. All values are presented as mean value  $\pm$  SD and statistical analyses were carried out using one-way analysis of variance (ANOVA) followed by Tukey's multiple comparison test (\*\*  $p < 0.01$ ).

### 2.2.6. Effect of Compound 4h on the Expression of p53

p53, a tumor suppressor gene, stops the formation of tumors. The activation of such a gene is known to be important in the regulation of the apoptotic pathway induced by various stimuli [35]. In order to understand the effect of TMP-based Schiff base **4h** on p53 dependent apoptotic pathway, the MDA-MB-231 cells were treated with compound **4h** at its IC<sub>50</sub> concentration for 24 h and the level of p53 was determined using ELISA assay. Figure 7 shows a rise in p53 levels of  $\sim 10.97$  fold when compared to the untreated control.

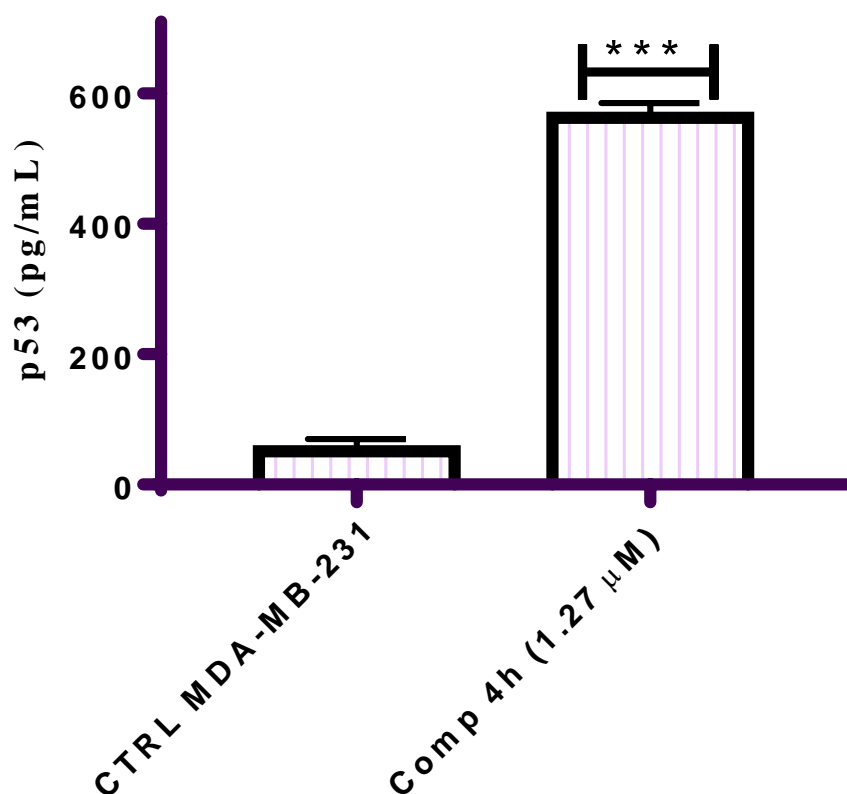


**Figure 7.** Graphical representation for the effect of Schiff base **4h** on the level of p53 in MDA-MB-231 cells for 24 h. All values are presented as mean value  $\pm$  SD and statistical analyses were carried out using one-way analysis of variance (ANOVA) followed by Tukey's multiple comparison test (\*\* $p < 0.001$ ).

### 2.2.7. Effect of Compound 4h on the Expression of Bax and Bcl-2

To further corroborate apoptosis induction by Schiff base **4h**, the level of anti-apoptotic protein (Bcl-2) and pro-apoptotic protein (Bax) was determined in vitro by ELISA in MDA-MB-231 cells treated with Schiff base **4h**. MDA-MB-231 cells were treated with compound **4h** at its IC<sub>50</sub> concentration for twenty-four hours. Compound **4h** decreased the amount of Bcl-2 in MDA-MB-231 cells by  $\sim 7.97$ -fold compared to untreated cells (Figure 8). Furthermore, compound **4h** increased the level of Bax by  $\sim 4.42$ -fold compared to untreated cells. As shown by apoptosis experiments, compound **4h** induces the intrinsic route of apoptosis by downregulating the levels of Bcl-2 and upregulating the levels of Bax.

### 2.2.8. Molecular Docking Study

A molecular docking study with tubulin was performed for *N*-3,5-dibromo-4-hydroxy-benzylidene hydrazinyl molecule **4h** into the active site of tubulin crystal structure (PDB: 1SA0) in order to reveal insight into its binding mode. A molecular docking simulation of compound **4h** into the tubulin protein binding site was performed using molecular operating environment (MOE) software, 2015.10. The docking results revealed that *N*-3,5-

dibromo-4-hydroxybenzylidene hydrazinyl molecule **4h** displayed good binding affinities ( $-25.49$  kcal/mol). In addition, *N*-3,5-dibromo-4-hydroxybenzylidene hydrazinyl molecule **4h** interacts with the active site of 1SA0 by three hydrogen bonds; Asn 101 with the oxygen of trimethoxyphenyl ring, Ser 140 with the oxygen atom of trimethoxy benzamide ring and Tyr 224 with the carbonyl oxygen of the amide group. Additionally, 3,5-dibromo-4-hydroxyphenyl ring formed  $\pi$ - $\pi$  interaction with Tyr 224 residue. These results reflect the higher activity and justify the experimental findings of compound **4h** (Figure 9).

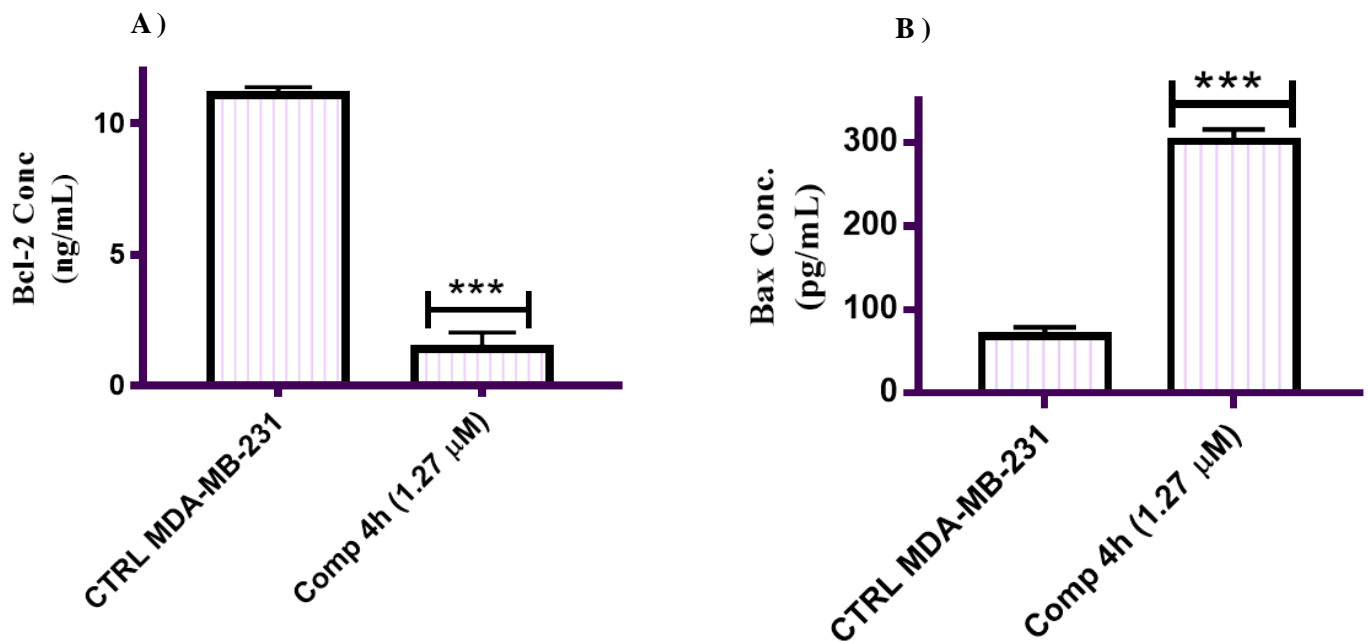


**Figure 8.** Graphical representation for the effect of Schiff base **4h** on the level of Bcl-2 and Bax in MDA-MB-231 cells for 24 h. (A) Effect on Bcl-2 level. (B) Effect on Bax level. All values are presented as mean value  $\pm$  SD and statistical analyses were carried out using one-way analysis of variance (ANOVA) followed by Tukey's multiple comparison test (\*\*\*)  $p < 0.001$ .

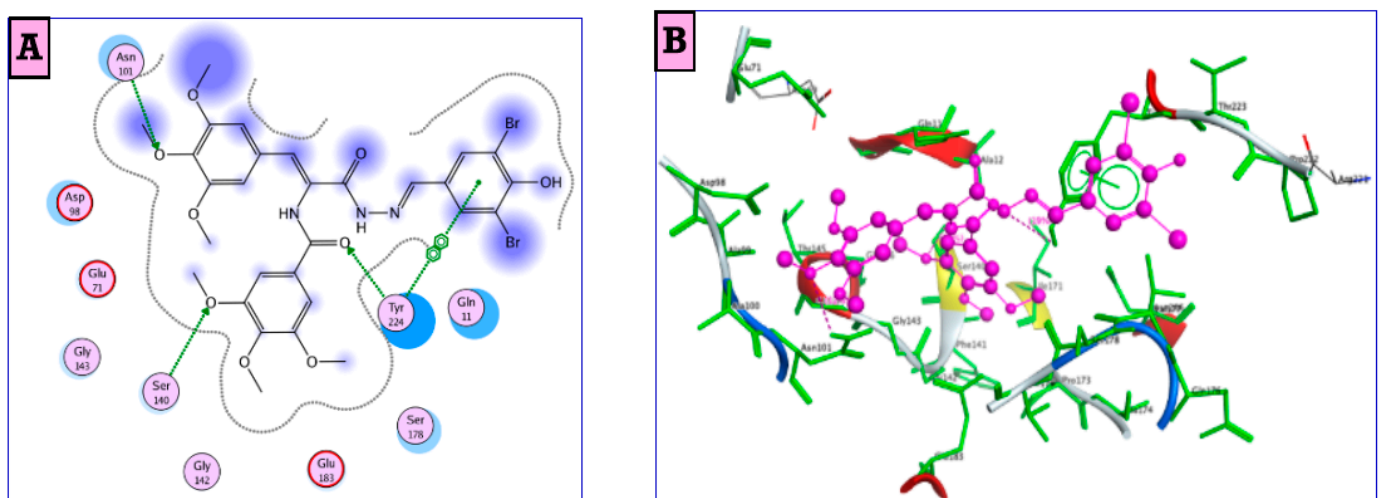


**Figure 9.** (A) show the 2D interactions of Schiff base **4h** into tubulin active site (PDB code: 1SA0). (B) show the 3D interactions of Schiff base **4h** into tubulin active site (PDB code: 1SA0).

### 2.3. Nanostructured Lipid Carrier Fabrication Studies

Aiming to enhance the pharmacokinetic characteristics as very poor aqueous solubility estimated utilizing free web-based tool Swiss ADME (<http://www.swissadme.ch/> accessed on 10 April 2022). Remarkably, the anticipated poor water-solubility of **4h** was ( $\text{LogS}_{\text{SILICOS-IT}} = 6.7 \times 10^{-7} \text{ mg/mL}; 9.27 \times 10^{-10} \text{ mol/L}$ ) which will impede its cytotoxic activity and possible clinical outcomes of compound **4h** (Figure 10). Thus, Nanostructured lipid carriers (NLCs) fabrication was proposed as a simple and economic tactic for boosting the kinetic properties of compound **4h**. NLCs aspired to promote the absorption of the compound besides improving its therapeutic response and reduce its predicted side effects. The composition of the eNLC matrix encompasses a blend of lipid molecules of various configurations, originally a gathering of both solid and liquid lipid, which is predisposed to the creation of more crystalline imperfections which in turn grant a greater gap for drug molecules accommodation [36]. Moreover, those crystalline imperfections allow the promotion of drug charging capability, and the suppression of the expulsion of the drug on storage, besides the modulation of the drug release pattern which is correlated to the variation in the composition of the lipid matrix [37]. There are colloidal dispersions of solid lipid and hydrophilic surfactant in the SLN form. Owing to the exclusive characteristics of NLCs, such as minute size, huge surface area, and improved drug loading potentiality [37], thus, loading compound **4h** on NLCs was assumed to promote its cytotoxic activity via densifying its biological manifestations at the tumor site.

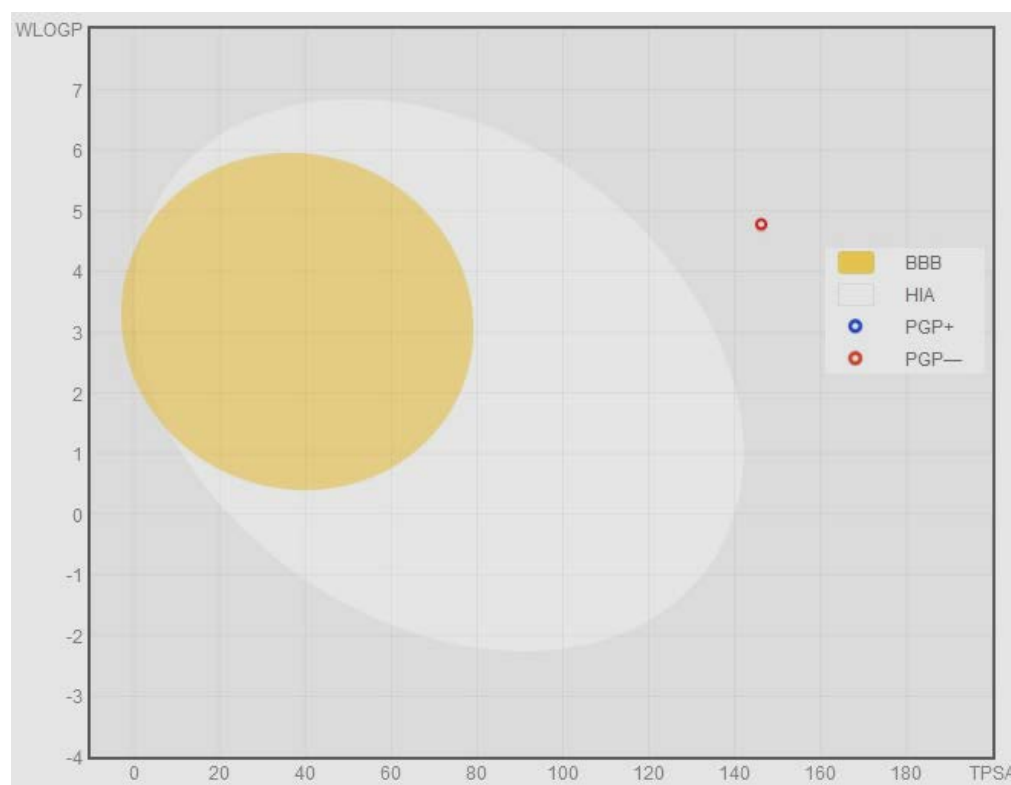


**Figure 10.** Human intestinal absorption (HIA) and blood-brain barrier (BBB) plot for **4h**.

### 2.4. Compound **4h** Loaded NLCs Design, Preparation and Optimization

Emulsification-ultrasonication technique was adopted for the fabrication of eight drug-loaded NLCs formulations. The design of the formulations was constructed via  $2^3$ -factorial design using Stat-Ease<sup>®</sup>-V.13 software (Design-Expert TM; Minneapolis, MN, USA) (Table 2). The picked independent variables were the type of lipid (A; X1), lipid concentration (B; X2), along with the concentration of surfactant (C; X3). The resulting 8 formulae were formulated, assessed for the pre-determined dependent responses: encapsulation efficiency, drug loading, and particle size.

sulation efficiency (Y1: EE%), particle size (Y2: PS) and zeta potential (Y4: ZP) and analyzed using Stat-Ease<sup>®</sup>- V.13 software. The compositions and the results of the dependent responses of eight drug-NLCs formulations were displayed in Table 2. Drug estimation at different concentrations was performed using HPLC at  $\lambda_{\max}$  254 nm [38].

**Table 2.** Experimental runs, independent variables, and estimated responses of 4h-loaded NLCs via 2<sup>3</sup> full factorial experimental.

Formula	A (Lipid Type)	B (Lipid Conc. %w/v)	C (Surfactant Conc. %w/v)	Y1 (EE%)	Y2 (PS)	Y3 (PDI)	Y4 (ZP)
F1	Precirol	2	1	80.9 ± 3.5	142.5 ± 12.2	0.34 ± 0.04	−24.6 ± 4.1
F2	Geleol	2	1	51.2 ± 2.8	311.2 ± 19.1	0.31 ± 0.05	−16.4 ± 1.2
F3	Precirol	6	1	95.6 ± 4.1	222.4 ± 11.7	0.23 ± 0.06	−39.2 ± 3.4
F4	Geleol	6	1	83.7 ± 4.6	354.3 ± 17.3	0.27 ± 0.05	−29.8 ± 2.2
F5	Precirol	2	2	54.3 ± 1.9	100.7 ± 8.1	0.54 ± 0.08	−18.3 ± 1.9
F6	Geleol	2	2	37.4 ± 1.8	253.4 ± 9.5	0.64 ± 0.17	−12.9 ± 1.8
F7	Precirol	6	2	86.8 ± 3.3	189.7 ± 12.6	0.36 ± 0.05	−31.2 ± 3.3
F8	Geleol	6	2	67.2 ± 2.4	269.5 ± 23.2	0.28 ± 0.02	21.7 ± 2.5

### 2.5. Fabrication Variables Influence on the Selected Responses

The characterization of the pre-determined responses for each drug-loaded formulae of NLCs: Entrapment Efficiency (Y1: EE%), particle size (Y2: PS) and zeta potential (Y3: ZP). From Table 2, it can be depicted that there was a discrepancy in the outcomes of the measured responses which denoted the great impact of the fabrication variables on the preselected NLCs characters.

The entrapment efficiency of the fabricated NLCs formula ranged from  $37.4 \pm 1.8$  for F6 to  $95.6 \pm 4.1$  for F3 and the impact of the variable's type of lipid (A; X1), lipid concentration (B; X2), along with the concentration of surfactant (C; X3) on EE% can be obviously displayed by the cubic plot and predicted versus actual values plots (Figure 11). Concerning the type of lipid (A), Precirol ATO-5 originated NLCs formulae exhibited significantly ( $p = 0.0065$ ) greater EE% values than those prepared utilizing Geleol. This may be attributed to the nature of the incorporated lipids which greatly affect the extent of creation of a well-organized crystalline lattice, where lipids enclosing fatty acid acyl glycerol of various chain length grants a higher space for the drug accommodation based on that they were able to configure a less organized particle [39]. Thus, Precirol ATO-5 constituted to form a mixture of various fatty acids of different chains (palmitic C16 and stearic C18) predisposes to a higher possibility to configure less ordered particles than that of Geleol (mono acid acyl glycerol), hence a higher gap for drug loading. Moreover, lipids that possess a blend of diverse chain fatty acids have a greater capability of drug solubilization, and hence, higher drug loading efficiency [40]. Moreover, increasing the lipid concentration (B; X2) from 2% to 6% results in a significant ( $p = 0.0019$ ) increase in EE%. This is plausible as a higher concentration of lipid means a greater amount of lipid was feasible to endorse drug molecules [41]. Meanwhile, increasing surfactant concentration (C; X3) resulted in subsequent significant ( $p = 0.0119$ ) reduction in EE%. The existence of surfactant results in a diminished interfacial tension between the aqueous phase and lipid phase predisposing to the production of particles of diminished size which in turn reduces the NLCs capacity to endorse higher amount of the drug [36,39].

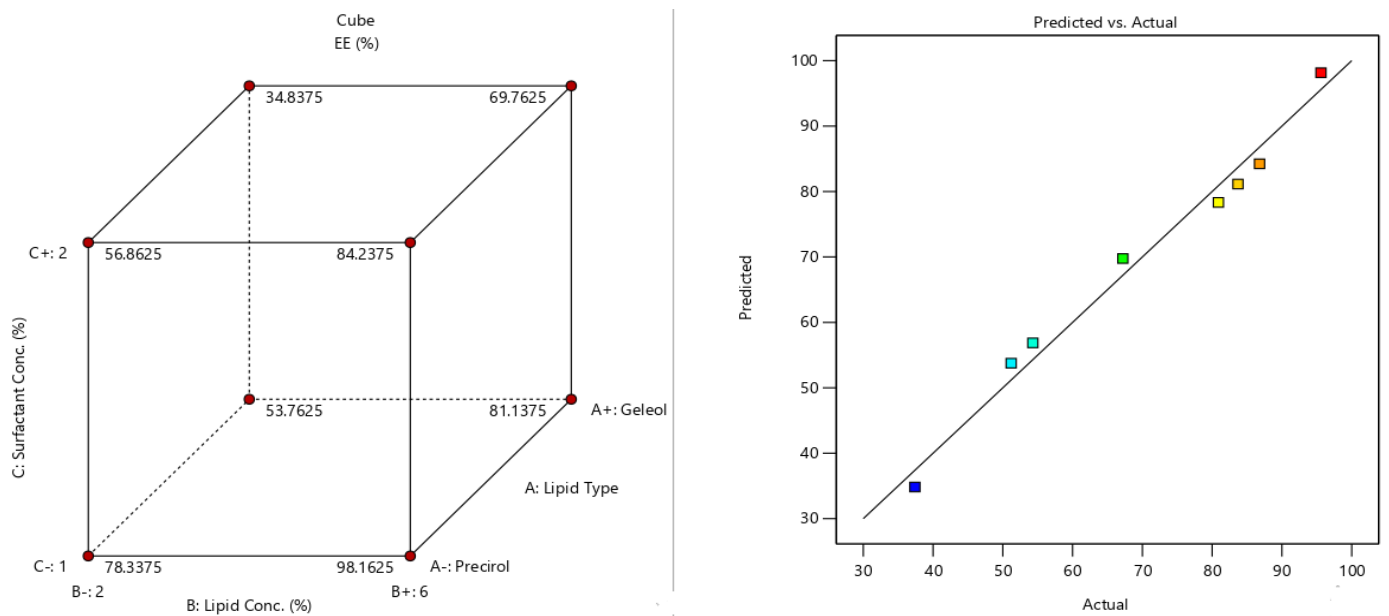


**Figure 11.** The impact of A: Lipid type, B: Lipid conc., C: surfactant conc. on EE percent of 4h-loaded NLC is represented in cubic plot and predicted versus actual values plot.

Concerning, PS (Y2) and PDI (Y3) of the formulated NLCs ranged from  $100.7 \pm 8.1$  nm to  $354.3 \pm 17.3$  and  $0.28 \pm 0.02$  to  $0.64 \pm 0.17$ , respectively. Figure 12 exposed the 3D surface plots variables type of lipid (A; X1), lipid concentration (B; X2), along with the concentration of surfactant (C; X3) and predicted versus actual values plots of PS. The PDI values give a clue on the degree of homogeneity or heterogeneity of the size of the investigated samples, where the PDI values on getting close to 1 affirm the heterogeneity of the sample and vice versa.

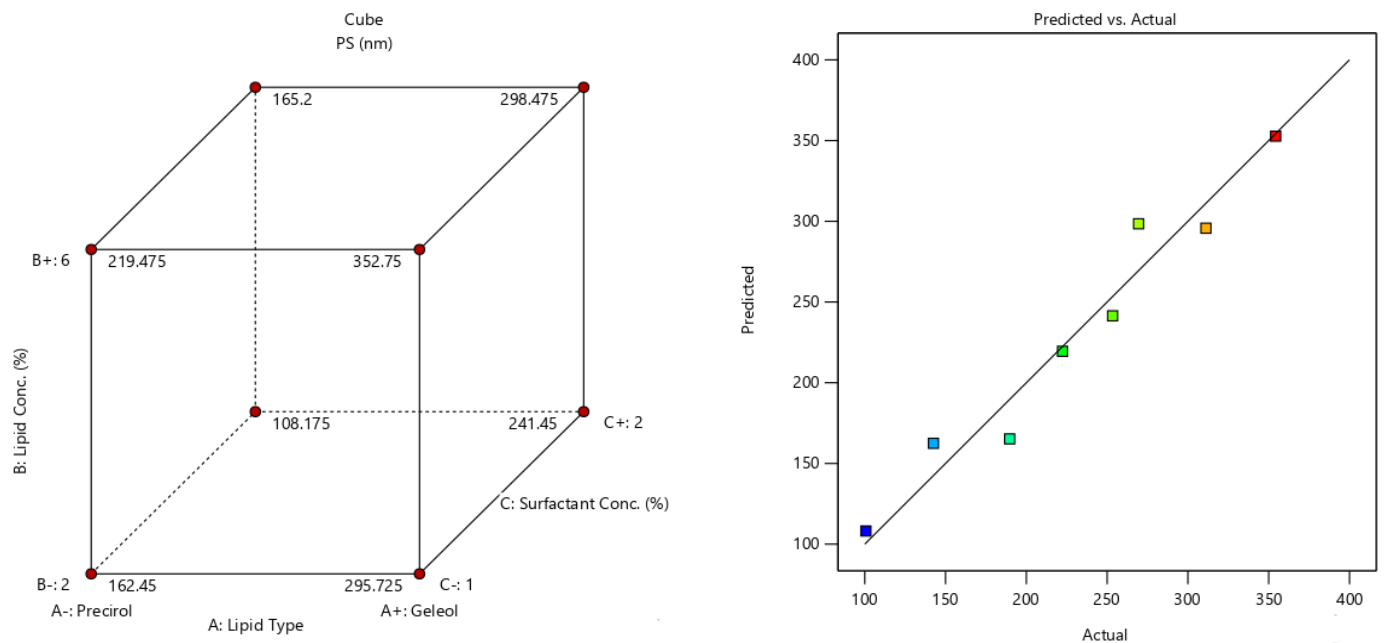


**Figure 12.** The impact of A: Lipid type, B: Lipid conc., C: surfactant conc. on PS of 4h-loaded NLC is represented in cubic plot and predicted versus actual values plot.

ANOVA results revealed that changing the type of lipid (A; X1) from Precirol ATO-5 to Geleol predisposed to a significant ( $p = 0.0014$ ) elevation in PS, owing to the fact that solid lipid possessing a higher melting point predisposed to gradual crystallization, and thus a higher opportunity to conform more organized crystals with larger particle size [42]. According to Das et al. who found that investigated particle size of formulated clotrimazole NLCs was highly affected by the alteration of type of lipids and following this descending order Compritol < Precirol < Geleol [36]. Moreover, increasing the lipid concentration (B; X2) from 2% to 6% results in significant ( $p = 0.028$ ) enlargement in PS, this may be attributed to the availability of a higher amount of lipids to enclose more drugs, thus increasing the PS. Moreover, increasing the amount of lipids will elevate the system viscosity which in turn will increase the tendency of particle aggregation [43]. On another hand, increasing the surfactant concentration significantly ( $p = 0.0326$ ) reduces the NLCs formulation PS. This can be justified owing to the fact that the increase in the concentration of surfactant will diminish lipid droplet surface tension, which will be able to be subdivided into a finer size. In addition, sufficient surfactant concentration will be able to wrap the minute lipid droplets and hinder their tendency to coalescence, thereby elevating the system stability [44].

Turning to ZP (Y4), its values ranged from  $-12.5 \pm 1.8$  to  $-39.2 \pm 3.4$  Mv denoting the higher stability of produced NLCs as the increase in ZP will subsequently positively affect the system stability. Figure 13 revealed the 3D surface plots variables type of lipid (A; X1), lipid concentration (B; X2), along with the concentration of surfactant (C; X3) and predicted versus actual values plots of ZP. From ANOVA results, it can be depicted that changing the type of lipid (A; X1) from Precirol ATO-5 to Geleol predisposed to a significant ( $p = 0.0021$ ) suppression in ZP and this came in accordance with Das et al., who revealed that the ZP values of the prepared SLN will increase in the following order: Geleol < Precirol < Compritol (1). This may be due to the higher negative charged groups associated with the blend of fatty acid incorporated in Precirol relative to the mono acid acyl in case of Geleol. However, increasing the lipid concentration led to a significant ( $p = 0.0004$ ) elevation in ZP values owing to the higher entrapment of drug-bearing anionic group within the particles, in addition to the increase in anionic groups of the fatty acids on increasing the lipid concentration [39]. Meanwhile, increasing the surfactant concentration significantly ( $p = 0.0048$ ) reduces the ZP values. the virtue of utilizing nonionic surfactant (Cremophore RH 40), which will not impart any additional charge besides the surfactant bulkiness, will aid in disguising the particles charge on surrounding it [39].

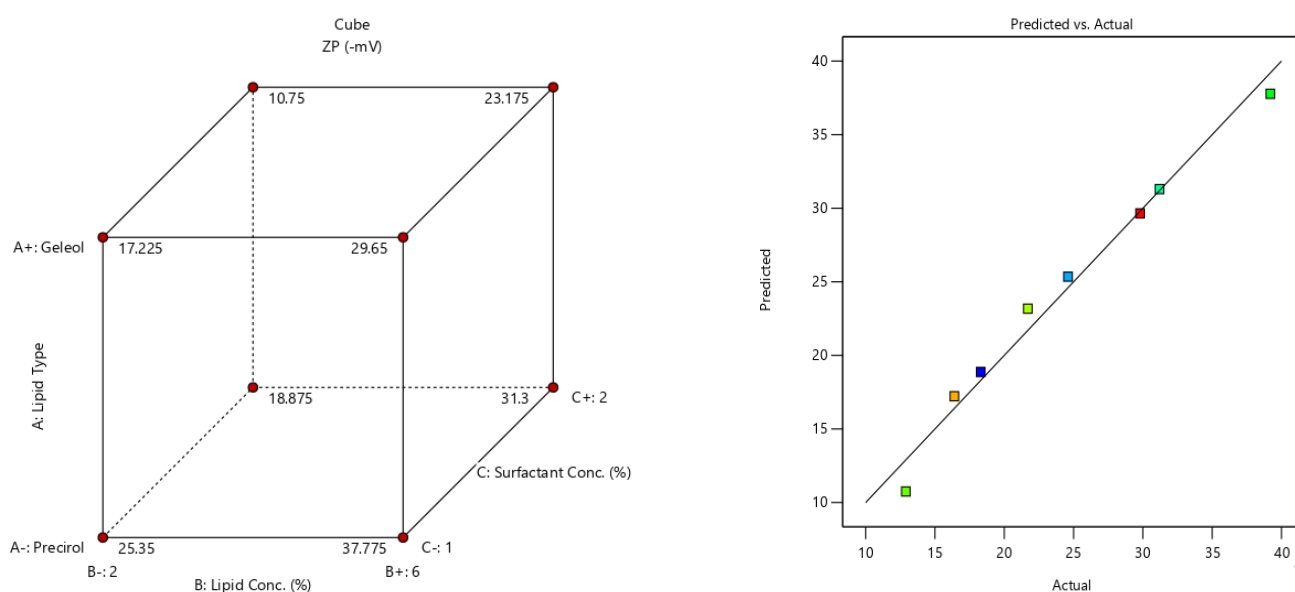


**Figure 13.** The impact of A: Lipid type, B: Lipid conc., C: surfactant conc. on ZP of 4h-loaded NLC is represented in cubic plot and predicted versus actual values plot.

## 2.6. Statistical Optimization of Fabrication Variables for Election the Optimum Formula

The optimization aimed to pick the best formula that possesses the predetermined criteria as maximum EE%, ZP and diminished PS. This was attained via analysis of the influence of the independent variables on the determined dependent criteria using The Design-Expert V.13 software. Based on  $2^3$  factorial design and its subsequent analysis F3 constituted of Precirol ATO 5 as lipid used in concentration 6% *w/v* along with 1% *w/v* Cremophore RH40 was chosen to be the optimum formula possessing a desirability value of 0.805. Moreover, as shown in Table 3 the predicted and actual values of EE%, PS and ZP were not gapped by more than 10% assuring the appropriateness of the design and the liability of its outcomes. (Figure 14) arise the optimum criteria for 4h-loaded NLCs.

**Table 3.**  $2^3$  factorial investigation outcome of 4h-loaded NLC and the predicted, observed responses and deviation percent of the Optimum formula (F3).

Responses	EE(%)	PS (nm)	ZP (Mv)
$R^2$	0.961	0.954	0.981
Adjusted $R^2$	0.93	0.92	0.966
Predicted $R^2$	0.845	0.818	0.92
Adequate precision	16.9	14.5	23.6
Significant factors	A, B, C	A, B, C	A, B, C
Observed value of the optimal formula (F3)	95.6	222.4	−39.2
Predicted value of the optimal formula (F3)	95.7	200.6	−35.5
Absolute deviation %	0.1	9.8	9.4

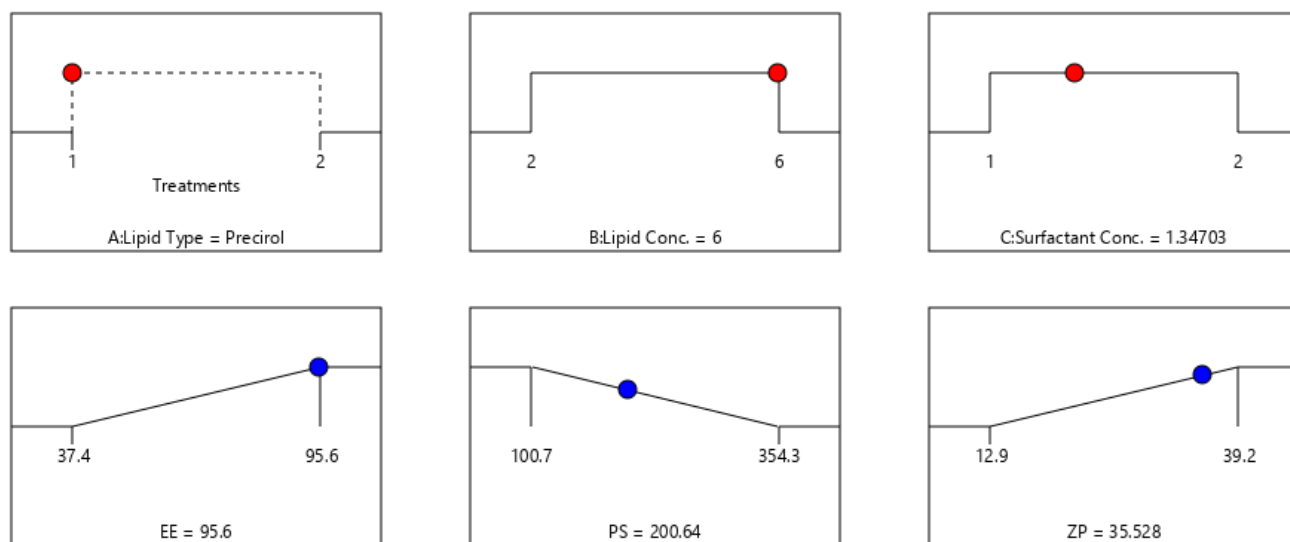


**Figure 14.** Optimization ramps for the examined independent variables utilize the optimal criteria of the formulation variables for 4h-loaded NLC formulas with the projected value of each measured formulation parameter.

## 2.7. In Vitro Assessment of the Optimum 4h-Loaded NLC

### 2.7.1. Particle Morphology Analysis via TEM

(Figure 15) displayed the attained image of the optimum 4h-loaded NLC formula (F3) using the TEM technique. It can be depicted as the spherical soft-shaped lipid nanoparticles devoid from any crystals for the drug.



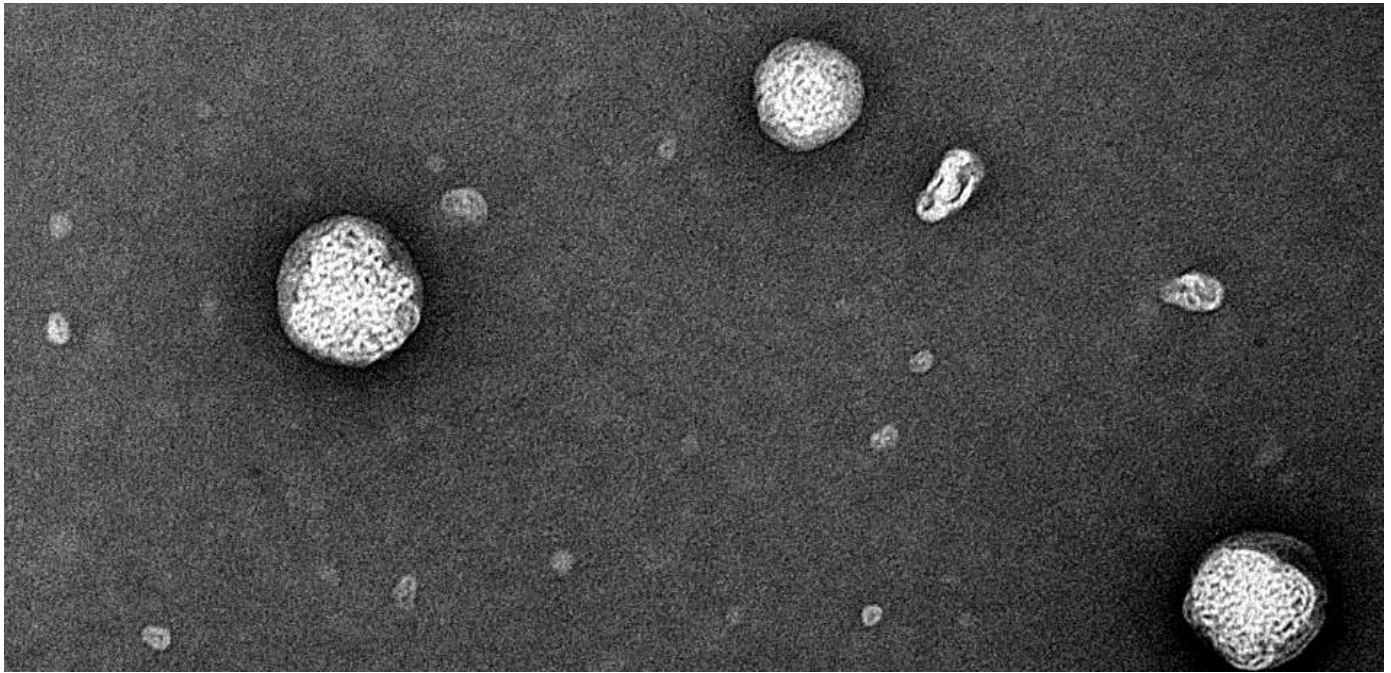


Figure 15. TEM of the picked optimized NLC formula.

#### 2.7.2. In Vitro Drug Release Experiment

The release attitude of the drug from drug-loaded NLC relative to drug suspension was conducted by adopting in vitro drug release experiment. The cumulative amount of drug released over 24 h was computed and found to be  $92.45\% \pm 3.37$  compared to  $20.8\% \pm 1.2$  for 4h suspension (Figure 16). Thus, NLCs as a carrier for the drug will aid in the extended release of the drug and its densifying in the tumor location in a more solubilized form [38].

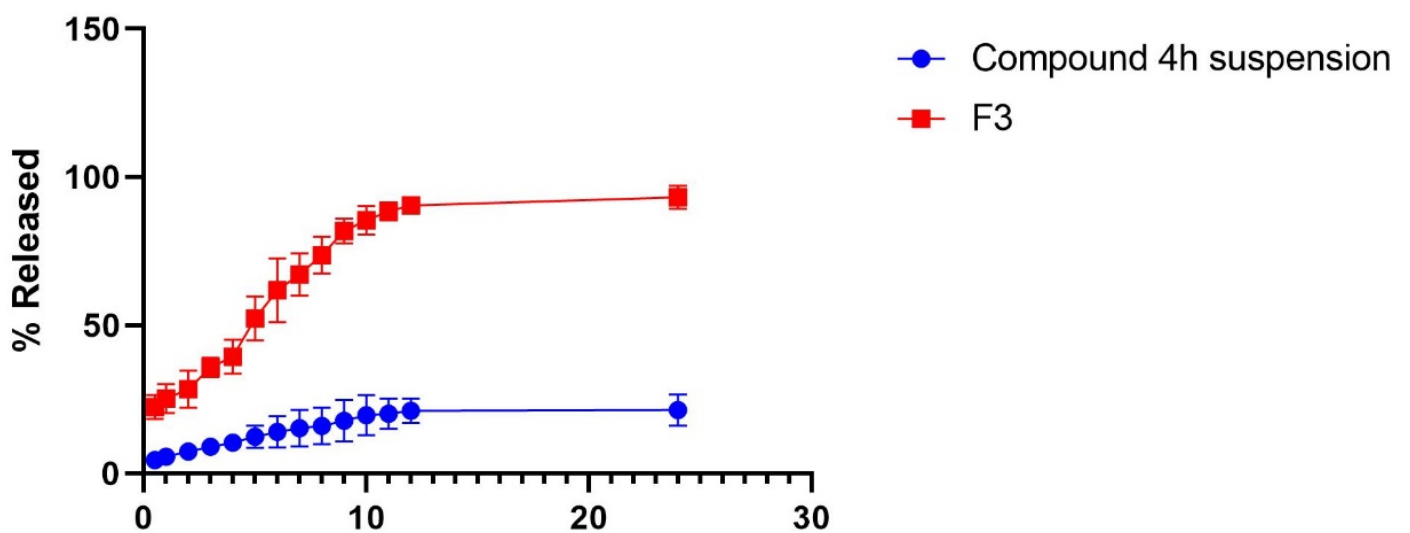
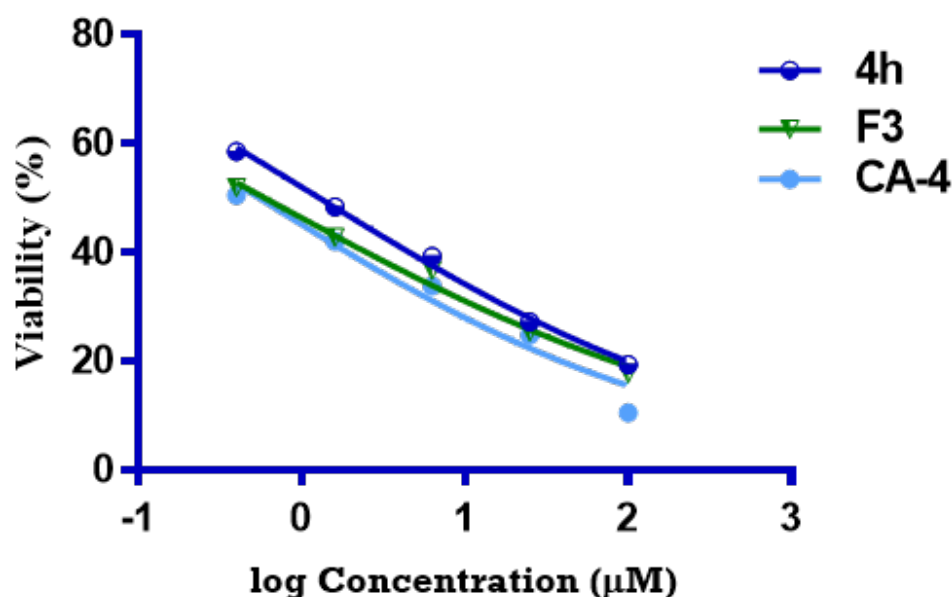


Figure 16. % of compound 4h released  $\pm$  S.D. from the optimized NLC (F3) compared to that of 4h suspensions.

### 2.7.3. Comparative Cytotoxicity Study of Optimized Formula versus Pure 4h

In order to highlight the significance of the drug lodging on NLCs, the cytotoxicity study was conducted for optimized NLCs (F3) relative to the pure drug. (Figure 17) revealed the % viability of MDA-MB-231 cancer cells post-exposure to both preparations and reference drugs. The  $IC_{50}$  values of the results were displayed in F3, pure 4h and CA-4 were ( $0.59 \pm 0.07$ ,  $1.27 \pm 0.18$  and  $0.54 \pm 0.04 \mu\text{M}$ ), respectively. The magnitude of cytotoxicity was found to increase on the following trend: compound 4h < F3 < CA-4. F3 exhibited the chief cytotoxicity over 4h and this may be attributed to the large surface area of NLCs, promoted drug solubility and release along with the promotion of the drug cellular uptake, all of these lead to a boost in the anticancer activity.



**Figure 17.** The graphical pattern showing the results of % cell viability of F3 versus 4h and CA-4 as reference drug at multiple concentrations ( $\mu\text{M}$ ) on MDA-MB-231 cancer cells.

## 3. Materials and Methods

### 3.1. General

See Supplementary Materials—Appendix SA.

### 3.2. Chemistry

#### 3.2.1. General Procedure for the Preparation of N-((Z)-3-((E)-2-(Ethylidene, furo or aryl)hydrazinyl)-3-oxo-1-(3,4,5-trimethoxyphenyl)prop-1-en-2-yl)-3,4,5-trimethoxybenzamides (2–4I)

Hydrazide 1 (0.46 g, 1 mmol) was added to a solution of an appropriate aldehyde; namely acetaldehyde, furfural or respective aryl aldehyde (1 mmol) in absolute ethanol (20 mL) containing a catalytic amount of acetic acid glacial (1 mL). The reaction mixture was refluxed for 6–8 h and then filtered. The residue obtained was dried, and crystallized from absolute ethanol to yield pure compounds 2, 3 and 4a–I.

#### N-((Z)-3-((E)-2-Ethylidenehydrazinyl)-3-oxo-1-(3,4,5-trimethoxyphenyl)prop-1-en-2-yl)-3,4,5-trimethoxybenzamide (2)

White powder (0.31 g, 63.92%), m.p. 224–226 °C.  $^1\text{H-NMR}$  (400 MHz,  $\text{DMSO-}d_6$ ,  $\delta$  ppm): 1.89 (s, 3H,  $\text{CH}_3$ ), 3.64 (s, 6H,  $2\text{OCH}_3$ ), 3.66 (s, 3H,  $\text{OCH}_3$ ), 3.73 (s, 3H,  $\text{OCH}_3$ ), 3.83 (s, 6H,  $2\text{OCH}_3$ ), 6.98 (s, 2H, arom.CH), 7.28 (s, 1H, olefinic CH), 7.40 (s, 2H, arom.CH), 9.85 (s, 1H,  $\text{CH}=\text{N}$ ), 9.89 (s, 1H, NH), 10.00 (s, 1H, NH).  $^{13}\text{C-NMR}$  (100 MHz,  $\text{DMSO-}d_6$ ,  $\delta$  ppm): 21.08 ( $\text{CH}_3$ ), 56.07 ( $2\text{OCH}_3$ ), 56.54 ( $2\text{OCH}_3$ ), 60.52 ( $\text{OCH}_3$ ), 60.64 ( $\text{OCH}_3$ ),

105.99 (C2,6 trimethoxyphenyl), 107.64 (C2,6 trimethoxyphenyl), 128.43 (C olefinic), 129.17 (C1 trimethoxyphenyl), 129.71 (C olefinic), 130.86 (C1 trimethoxybenzamide), 138.58 (C4 trimethoxyphenyl), 140.87 (C4 trimethoxybenzamide), 152.95 (C3,5 trimethoxyphenyl), 153.04 (C3,5 trimethoxybenzamide), 164.60 (C=N), 165.73 (C=O trimethoxybenzamide), 168.55 (C=O hydrazide). Anal. Calcd. for C<sub>24</sub>H<sub>29</sub>N<sub>3</sub>O<sub>8</sub> (487.50): C, 59.13; H, 6.00; N, 8.62. Found: C, 59.24; H, 6.06; N, 8.67.

N-((Z)-3-((E)-2-(Furan-2-ylmethylene)hydrazinyl)-3-oxo-1-(3,4,5-trimethoxyphenyl)prop-1-en-2-yl)-3,4,5-trimethoxybenzamide (**3**)

White powder (0.39 g, 71.82%), m.p. 212–214 °C. <sup>1</sup>H-NMR (400 MHz, DMSO-*d*<sub>6</sub>, δ ppm): 3.66 (s, 6H, 2OCH<sub>3</sub>), 3.68 (s, 3H, OCH<sub>3</sub>), 3.74 (s, 3H, OCH<sub>3</sub>), 3.84 (s, 6H, 2OCH<sub>3</sub>), 6.64 (s, 1H, furan CH), 6.90 (d, *J* = 3.0 Hz, 1H, furan CH), 7.03 (s, 2H, arom.CH), 7.21 (s, 1H, olefinic CH), 7.44 (s, 2H, arom.CH), 7.85 (s, 1H, furan CH), 8.35 (s, 1H, CH=N), 10.03 (s, 1H, NH), 11.58 (s, 1H, NH). <sup>13</sup>C-NMR (100 MHz, DMSO-*d*<sub>6</sub>, δ ppm): 56.10 (2OCH<sub>3</sub>), 56.56 (2OCH<sub>3</sub>), 60.56 (OCH<sub>3</sub>), 60.66 (OCH<sub>3</sub>), 105.97 (C2,6 trimethoxyphenyl), 107.79 (C2,6 trimethoxybenzamide), 112.65 (C4 furan), 113.74 (C3 furan), 128.81 (C olefinic), 129.14 (C1 trimethoxyphenyl), 129.79 (C olefinic), 129.93 (C1 trimethoxybenzamide), 137.75 (C=N), 138.64 (C4 trimethoxyphenyl), 141.06 (C4 trimethoxybenzamide), 145.60 (C5 furan), 150.03 (C2 furan), 153.07 (C3,5 trimethoxyphenyl and C3,5 trimethoxybenzamide), 162.48 (C=O trimethoxybenzamide), 165.68 (C=O hydrazide). Anal. Calcd. for C<sub>27</sub>H<sub>29</sub>N<sub>3</sub>O<sub>9</sub> (539.53): C, 60.11; H, 5.42; N, 7.79. Found: C, 60.03; H, 5.45; N, 7.86.

N-((Z)-3-((E)-2-(4-Fluorobenzylidene)hydrazinyl)-3-oxo-1-(3,4,5-trimethoxyphenyl)prop-1-en-2-yl)-3,4,5-trimethoxybenzamide (**4a**)

White powder (0.43 g, 75.03%), m.p. 201–203 °C. <sup>1</sup>H-NMR (400 MHz, DMSO-*d*<sub>6</sub>, δ ppm): 3.67 (s, 6H, 2OCH<sub>3</sub>), 3.68 (s, 3H, OCH<sub>3</sub>), 3.74 (s, 3H, OCH<sub>3</sub>), 3.84 (s, 6H, 2OCH<sub>3</sub>), 7.03 (s, 2H, arom.CH), 7.21 (s, 1H, olefinic CH), 7.30 (t, *J* = 8.6 Hz, 2H, arom.CH), 7.45 (s, 2H, arom.CH), 7.73–7.83 (m, 2H, arom.CH), 8.44 (s, 1H, CH=N), 10.05 (s, 1H, NH), 11.66 (s, 1H, NH). <sup>13</sup>C-NMR (400 MHz, DMSO-*d*<sub>6</sub>, δ ppm): 56.11 (2OCH<sub>3</sub>), 56.56 (2OCH<sub>3</sub>), 60.56 (OCH<sub>3</sub>), 60.65 (OCH<sub>3</sub>), 105.97 (C2,6 trimethoxyphenyl), 107.80 (C2,6 trimethoxybenzamide), 116.27 (C3 fluorophenyl), 116.49 (C5 fluorophenyl), 128.79 (C olefinic), 129.19 (C1 trimethoxyphenyl), 129.57 (C olefinic), 129.66 (C1 trimethoxybenzamide), 129.78 (C1 fluorophenyl), 129.87 (C2 fluorophenyl), 131.49 (C6 fluorophenyl), 138.65 (C4 trimethoxyphenyl), 141.06 (C4 trimethoxybenzamide), 146.80 (C=N), 153.08 (C3,5 trimethoxyphenyl and C3,5 trimethoxybenzamide), 162.30 (C4 fluorophenyl), 162.59 (C=O trimethoxybenzamide), 165.72 (C=O hydrazide). Anal. Calcd. for C<sub>29</sub>H<sub>30</sub>FN<sub>3</sub>O<sub>8</sub> (567.56): C, 61.37; H, 5.33; N, 7.40. Found: C, 61.24; H, 5.36; N, 7.35.

N-((Z)-3-((E)-2-(4-Chlorobenzylidene)hydrazinyl)-3-oxo-1-(3,4,5-trimethoxyphenyl)prop-1-en-2-yl)-3,4,5-trimethoxybenzamide (**4b**)

White powder (0.40 g, 69.14%), m.p. 233–235 °C. <sup>1</sup>H-NMR (400 MHz, DMSO-*d*<sub>6</sub>, δ ppm): 3.66 (s, 6H, 2OCH<sub>3</sub>), 3.67 (s, 3H, OCH<sub>3</sub>), 3.73 (s, 3H, OCH<sub>3</sub>), 3.83 (s, 6H, 2OCH<sub>3</sub>), 7.03 (s, 2H, arom.CH), 7.20 (s, 1H, olefinic CH), 7.44 (s, 2H, arom.CH), 7.52 (d, *J* = 8.1 Hz, 2H, arom.CH), 7.73 (d, *J* = 8.2 Hz, 2H, arom.CH), 8.43 (s, 1H, CH=N), 10.05 (s, 1H, NH), 11.70 (s, 1H, NH). <sup>13</sup>C-NMR (400 MHz, DMSO-*d*<sub>6</sub>, δ ppm): 56.12 (2OCH<sub>3</sub>), 56.57 (2OCH<sub>3</sub>), 60.57 (OCH<sub>3</sub>), 60.65 (OCH<sub>3</sub>), 105.98 (C2,6 trimethoxyphenyl), 107.82 (C2,6 trimethoxybenzamide), 128.78 (C olefinic), 129.07 (C3,5 chlorophenyl), 129.42 (C2,6 chlorophenyl), 129.76 (C1 trimethoxyphenyl), 129.92 (C olefinic), 133.87 (C1 trimethoxybenzamide), 134.86 (C1 chlorophenyl), 138.66 (C4 chlorophenyl), 141.07 (C4 trimethoxyphenyl), 143.81 (C4 trimethoxybenzamide), 146.54 (C=N), 153.08 (C3,5 trimethoxyphenyl and C3,5 trimethoxybenzamide), 162.63 (C=O trimethoxybenzamide), 165.70 (C=O hydrazide). Anal. Calcd. for C<sub>29</sub>H<sub>30</sub>ClN<sub>3</sub>O<sub>8</sub> (584.02): C, 59.64; H, 5.18; N, 7.20. Found: C, 59.86; H, 5.30; N, 7.44.

3,4,5-Trimethoxy-N-((Z)-3-((E)-2-(2-nitrobenzylidene)hydrazinyl)-3-oxo-1-(3,4,5-trimethoxyphenyl)prop-1-en-2-yl)benzamide (**4c**)

White powder (0.35 g, 58.92%), m.p. 239–241 °C. <sup>1</sup>H-NMR (400 MHz, DMSO-*d*<sub>6</sub>, δ ppm): 3.69 (s, 9H, 3OCH<sub>3</sub>), 3.75 (s, 3H, OCH<sub>3</sub>), 3.85 (s, 6H, 2OCH<sub>3</sub>), 7.06 (s, 2H, arom.CH), 7.23 (s, 1H, olefinic CH), 7.46 (s, 2H, arom.CH), 7.69 (t, *J* = 7.5 Hz, 1H, arom.CH), 7.82 (d, *J* = 7.0 Hz, 1H, arom.CH), 8.08 (d, *J* = 7.9 Hz, 1H, arom.CH), 8.13 (d, *J* = 7.5 Hz, 1H, arom.CH), 8.85 (s, 1H, CH=N), 10.10 (s, 1H, NH), 12.02 (s, 1H, NH). <sup>13</sup>C-NMR (400 MHz, DMSO-*d*<sub>6</sub>, δ ppm): 56.14 (2OCH<sub>3</sub>), 56.57 (2OCH<sub>3</sub>), 60.57 (OCH<sub>3</sub>), 60.66 (OCH<sub>3</sub>), 105.97 (C2,6 trimethoxyphenyl), 107.88 (C2,6 trimethoxybenzamide), 125.08 (C3 nitrophenyl), 128.35 (C olefinic), 128.69 (C1 trimethoxyphenyl), 129.00 (C olefinic), 129.31 (C1 nitrophenyl), 129.70 (C1 trimethoxybenzamide), 130.19 (C6 nitrophenyl), 131.02 (C4 nitrophenyl), 134.16 (C5 nitrophenyl), 141.11 (C4 trimethoxyphenyl), 142.78 (C4 trimethoxybenzamide), 148.71 (C=N), 153.10 (C3,5 trimethoxyphenyl), 153.11 (C3,5 trimethoxybenzamide), 162.89 (C=O trimethoxybenzamide), 164.69 (C2 nitrophenyl), 165.76 (C=O hydrazide). Anal. Calcd. for C<sub>29</sub>H<sub>30</sub>N<sub>4</sub>O<sub>10</sub> (594.57): C, 58.58; H, 5.09; N, 9.42. Found: C, 58.39; H, 5.12; N, 9.37.

N-((Z)-3-((E)-2-(2-Hydroxybenzylidene)hydrazinyl)-3-oxo-1-(3,4,5-trimethoxyphenyl)prop-1-en-2-yl)-3,4,5-trimethoxybenzamide (**4d**)

White powder (0.35 g, 61.17%), m.p. 220–222 °C. <sup>1</sup>H-NMR (400 MHz, DMSO-*d*<sub>6</sub>, δ ppm): 3.67 (s, 6H, 2OCH<sub>3</sub>), 3.68 (s, 3H, OCH<sub>3</sub>), 3.75 (s, 3H, OCH<sub>3</sub>), 3.85 (s, 6H, 2OCH<sub>3</sub>), 6.93 (t, *J* = 8.2 Hz, 2H, arom.CH), 7.04 (s, 2H, arom.CH), 7.27 (s, 1H, olefinic CH), 7.28–7.34 (m, 1H, arom.CH), 7.46 (s, 2H, arom.CH), 7.51 (d, *J* = 7.4 Hz, 1H, arom.CH), 8.63 (s, 1H, CH=N), 10.07 (s, 1H, NH), 11.32 (s, 1H, OH), 11.89 (s, 1H, NH). <sup>13</sup>C-NMR (100 MHz, DMSO-*d*<sub>6</sub>, δ ppm): 56.12 (2OCH<sub>3</sub>), 56.58 (2OCH<sub>3</sub>), 60.57 (OCH<sub>3</sub>), 60.67 (OCH<sub>3</sub>), 106.00 (C2,6 trimethoxyphenyl), 107.85 (C2,6 trimethoxybenzamide), 116.87 (C3 hydroxyphenyl), 119.19 (C1 hydroxyphenyl), 119.81 (C5 hydroxyphenyl), 128.70 (C olefinic), 128.75 (C1 trimethoxyphenyl), 129.68 (C6 hydroxyphenyl), 129.95 (C olefinic), 130.39 (C1 trimethoxybenzamide), 131.76 (C4 hydroxyphenyl), 138.76 (C4 trimethoxyphenyl), 141.10 (C4 trimethoxybenzamide), 148.57 (C=N), 153.09 (C3,5 trimethoxyphenyl and C3,5 trimethoxybenzamide), 157.90 (C2 hydroxyphenyl), 162.31 (C=O trimethoxybenzamide), 165.75 (C=O hydrazide). Anal. Calcd. for C<sub>29</sub>H<sub>31</sub>N<sub>3</sub>O<sub>9</sub> (565.57): C, 61.59; H, 5.52; N, 7.43. Found: C, 61.87; H, 5.54; N, 7.47.

N-((Z)-3-((E)-2-(4-Hydroxybenzylidene)hydrazinyl)-3-oxo-1-(3,4,5-trimethoxyphenyl)prop-1-en-2-yl)-3,4,5-trimethoxybenzamide (**4e**)

White powder (0.31 g, 54.27%), m.p. 255–257 °C. <sup>1</sup>H-NMR (400 MHz, DMSO-*d*<sub>6</sub>, δ ppm): 3.68 (s, 3H, OCH<sub>3</sub>), 3.68 (s, 6H, 2OCH<sub>3</sub>), 3.74 (s, 3H, OCH<sub>3</sub>), 3.84 (s, 6H, 2OCH<sub>3</sub>), 7.05 (s, 2H, arom.CH), 7.23 (s, 1H, olefinic CH), 7.45 (s, 2H), 7.97 (d, *J* = 7.9 Hz, 2H, arom.CH), 8.31 (d, *J* = 7.9 Hz, 2H, arom.CH), 8.55 (s, 1H, CH=N), 10.10 (s, 1H, NH), 11.95 (s, 1H, NH). <sup>13</sup>C-NMR (100 MHz, DMSO-*d*<sub>6</sub>, δ ppm): 56.13 (2OCH<sub>3</sub>), 56.57 (2OCH<sub>3</sub>), 60.58 (OCH<sub>3</sub>), 60.66 (OCH<sub>3</sub>), 105.97 (C2,6 trimethoxyphenyl), 107.88 (C2,6 trimethoxybenzamide), 124.57 (C olefinic), 128.35 (C3,5 hydroxyphenyl), 128.69 (C1 trimethoxyphenyl and C1 trimethoxybenzamide), 129.68 (C olefinic), 133.69 (C1 hydroxyphenyl), 138.75 (C2,6 hydroxyphenyl), 138.89 (C4 trimethoxyphenyl), 141.24 (C4 trimethoxybenzamide), 145.33 (C=N), 151.73 (C4 hydroxyphenyl), 153.10 (C3,5 trimethoxyphenyl and C3,5 trimethoxybenzamide), 163.18 (C=O trimethoxybenzamide), 165.74 (C=O hydrazide). Anal. Calcd. for C<sub>29</sub>H<sub>31</sub>N<sub>3</sub>O<sub>9</sub> (565.57): C, 61.59; H, 5.52; N, 7.43. Found: C, 61.43; H, 5.56; N, 7.58.

3,4,5-Trimethoxy-N-((Z)-3-((E)-2-(4-methylbenzylidene)hydrazinyl)-3-oxo-1-(3,4,5-trimethoxyphenyl)prop-1-en-2-yl)benzamide (**4f**)

White powder (0.40 g, 70.38%), m.p. 208–210 °C. <sup>1</sup>H-NMR (400 MHz, DMSO-*d*<sub>6</sub>, δ ppm): 2.35 (s, 3H, CH<sub>3</sub>), 3.67 (s, 6H, 2OCH<sub>3</sub>), 3.68 (s, 3H, OCH<sub>3</sub>), 3.74 (s, 3H, OCH<sub>3</sub>), 3.84

(s, 6H, 2OCH<sub>3</sub>), 7.03 (s, 2H, arom.CH), 7.21 (s, 1H, olefinic CH), 7.28 (d, *J* = 7.8 Hz, 2H, arom.CH), 7.45 (s, 2H, arom.CH), 7.61 (d, *J* = 7.8 Hz, 2H, arom.CH), 8.41 (s, 1H, CH=N), 10.04 (s, 1H, NH), 11.57 (s, 1H, NH). <sup>13</sup>C-NMR (100 MHz, DMSO-*d*<sub>6</sub>, δ ppm): 21.50 (CH<sub>3</sub>), 56.11 (2OCH<sub>3</sub>), 56.56 (2OCH<sub>3</sub>), 60.56 (OCH<sub>3</sub>), 60.65 (OCH<sub>3</sub>), 105.98 (C2,6 trimethoxyphenyl), 107.79 (C2,6 trimethoxybenzamide), 127.44 (C2,6 methylphenyl), 128.83 (C olefinic), 129.28 (C1 trimethoxyphenyl), 129.74 (C olefinic), 129.82 (C1 trimethoxybenzamide), 129.92 (C3,5 methylphenyl), 132.20 (C1 methylphenyl), 138.61 (C4 trimethoxyphenyl), 140.27 (C4 methylphenyl), 141.05 (C4 trimethoxybenzamide), 147.97 (C=N), 153.07 (C3,5 trimethoxyphenyl and C3,5 trimethoxybenzamide), 162.47 (C=O trimethoxybenzamide), 165.69 (C=O hydrazide). Anal. Calcd. for C<sub>30</sub>H<sub>33</sub>N<sub>3</sub>O<sub>8</sub> (563.60): C, 63.93; H, 5.90; N, 7.46. Found: C, 63.72; H, 5.78; N, 7.57.

3,4,5-Trimethoxy-N-((Z)-3-((E)-2-(4-methoxybenzylidene)hydrazinyl)-3-oxo-1-(3,4,5-trimethoxyphenyl)prop-1-en-2-yl)benzamide (**4g**)

White powder (0.37 g, 64.51%), m.p. 217–219 °C. <sup>1</sup>H-NMR (400 MHz, DMSO-*d*<sub>6</sub>, δ ppm): 3.66 (s, 6H, 2OCH<sub>3</sub>), 3.68 (s, 3H, OCH<sub>3</sub>), 3.74 (s, 3H, OCH<sub>3</sub>), 3.82 (s, 3H, OCH<sub>3</sub>), 3.84 (s, 6H, 2OCH<sub>3</sub>), 7.03 (d, *J* = 5.5 Hz, 4H, arom.CH), 7.20 (s, 1H, olefinic CH), 7.45 (s, 2H, arom.CH), 7.65 (d, *J* = 8.5 Hz, 2H, arom.CH), 8.38 (s, 1H, CH=N), 10.02 (s, 1H, NH), 11.50 (s, 1H, NH). <sup>13</sup>C-NMR (100 MHz, DMSO-*d*<sub>6</sub>, δ ppm): 55.76 (OCH<sub>3</sub>), 56.10 (2OCH<sub>3</sub>), 56.56 (2OCH<sub>3</sub>), 60.56 (OCH<sub>3</sub>), 60.65 (OCH<sub>3</sub>), 105.98 (C2,6 trimethoxyphenyl), 107.77 (C2,6 trimethoxybenzamide), 114.82 (C3,5 methoxyphenyl), 127.46 (C1 methoxyphenyl), 128.86 (C olefinic), 129.05 (C2,6 methoxyphenyl), 129.33 (C olefinic), 129.67 (C1 trimethoxyphenyl), 129.86 (C1 trimethoxybenzamide), 138.59 (C4 trimethoxyphenyl), 141.04 (C4 trimethoxybenzamide), 147.85 (C=N), 153.07 (C3,5 trimethoxyphenyl and C3,5 trimethoxybenzamide), 161.24 (C4 methoxyphenyl), 162.35 (C=O trimethoxybenzamide), 165.68 (C=O hydrazide). Anal. Calcd. for C<sub>30</sub>H<sub>33</sub>N<sub>3</sub>O<sub>9</sub> (579.60): C, 62.17; H, 5.74; N, 7.25. Found: C, 61.99; H, 5.77; N, 7.28.

N-((Z)-3-((E)-2-(3,5-Dibromo-4-hydroxybenzylidene)hydrazinyl)-3-oxo-1-(3,4,5-trimethoxyphenyl)prop-1-en-2-yl)-3,4,5-trimethoxybenzamide (**4h**)

White powder (0.48 g, 66.03%), m.p. 198–200 °C. <sup>1</sup>H-NMR (400 MHz, DMSO-*d*<sub>6</sub>, δ ppm): 3.67 (s, 3H, OCH<sub>3</sub>), 3.68 (s, 6H, 2OCH<sub>3</sub>), 3.74 (s, 3H, OCH<sub>3</sub>), 3.84 (s, 6H, 2OCH<sub>3</sub>), 7.03 (s, 2H, arom.CH), 7.19 (s, 1H, olefinic CH), 7.44 (s, 2H, arom.CH), 7.88 (s, 2H, arom.CH), 8.29 (s, 1H, CH=N), 10.04 (s, 1H, NH), 10.43 (s, 1H, OH), 11.73 (s, 1H, NH). <sup>13</sup>C-NMR (100 MHz, DMSO-*d*<sub>6</sub>, δ ppm): 56.12 (2OCH<sub>3</sub>), 56.56 (2OCH<sub>3</sub>), 60.57 (2OCH<sub>3</sub>), 60.66 (OCH<sub>3</sub>), 105.96 (C2,6 trimethoxyphenyl), 107.81 (C2,6 trimethoxybenzamide), 112.70 (C3,5 dibromophenyl), 128.79 (C olefinic), 129.16 (C1 trimethoxyphenyl), 129.51 (C olefinic), 129.77 (C1 trimethoxybenzamide), 129.83 (C1 dibromophenyl), 130.97 (C2,6 dibromophenyl), 138.64 (C4 trimethoxyphenyl), 141.06 (C4 trimethoxybenzamide), 144.84 (C=N), 152.56 (C4 dibromophenyl), 153.08 (C3,5 trimethoxyphenyl and C3,5 trimethoxybenzamide), 162.63 (C=O trimethoxybenzamide), 165.69 (C=O hydrazide). Anal. Calcd. for C<sub>29</sub>H<sub>29</sub>Br<sub>2</sub>N<sub>3</sub>O<sub>9</sub> (723.36): C, 48.15; H, 4.04; N, 5.81. Found: C, 48.31; H, 4.01; N, 5.78.

N-((Z)-3-((E)-2-(4-(Dimethylamino)benzylidene)hydrazinyl)-3-oxo-1-(3,4,5-trimethoxyphenyl)prop-1-en-2-yl)-3,4,5-trimethoxybenzamide (**4i**)

White powder (0.37 g, 61.82%), m.p. 243–245 °C. <sup>1</sup>H-NMR (400 MHz, DMSO-*d*<sub>6</sub>, δ ppm): 2.98 (s, 6H, 2CH<sub>3</sub>), 3.66 (s, 6H, 2OCH<sub>3</sub>), 3.67 (s, 3H, OCH<sub>3</sub>), 3.74 (s, 3H, OCH<sub>3</sub>), 3.84 (s, 6H, 2OCH<sub>3</sub>), 6.76 (d, *J* = 8.7 Hz, 2H, arom.CH), 7.02 (s, 2H, arom.CH), 7.20 (s, 1H, olefinic CH), 7.44 (s, 2H, arom.CH), 7.52 (d, *J* = 8.7 Hz, 2H, arom.CH), 8.29 (s, 1H, CH=N), 10.00 (s, 1H, NH), 11.32 (s, 1H, NH). <sup>13</sup>C-NMR (100 MHz, DMSO-*d*<sub>6</sub>, δ ppm): 40.25 (2CH<sub>3</sub>), 56.09 (2OCH<sub>3</sub>), 56.56 (2OCH<sub>3</sub>), 60.55 (OCH<sub>3</sub>), 60.65 (OCH<sub>3</sub>), 105.99 (C2,6 trimethoxyphenyl), 107.72 (C2,6 trimethoxybenzamide), 112.31 (C3,5 dimethylaminophenyl), 122.20 (C1 dime-

thylaminophenyl), 128.79 (C2,6 dimethylaminophenyl), 128.95 (C olefinic), 129.46 (C1 trimethoxyphenyl), 129.48 (C olefinic), 129.94 (C1 trimethoxybenzamide), 138.52 (C4 trimethoxyphenyl), 141.01 (C4 trimethoxybenzamide), 148.83 (C=N), 151.94 (C4 dimethylaminophenyl), 153.05 (C3,5 trimethoxyphenyl and C3,5 trimethoxybenzamide), 162.02 (C=O trimethoxybenzamide), 165.66 (C=O hydrazide). Anal. Calcd. for C<sub>31</sub>H<sub>36</sub>N<sub>4</sub>O<sub>8</sub> (592.64): C, 62.83; H, 6.12; N, 9.45. Found: C, 62.64; H, 6.04; N, 9.41.

N-((Z)-3-((E)-2-(4-Hydroxy-3-methoxybenzylidene)hydrazinyl)-3-oxo-1-(3,4,5-trimethoxyphenyl)prop-1-en-2-yl)-3,4,5-trimethoxybenzamide (**4j**)

White powder (0.32 g, 54.08%), m.p. 226–228 °C. <sup>1</sup>H-NMR (400 MHz, DMSO-*d*<sub>6</sub>, δ ppm): 3.66 (s, 6H, 2OCH<sub>3</sub>), 3.68 (s, 3H, OCH<sub>3</sub>), 3.74 (s, 3H, OCH<sub>3</sub>), 3.81 (s, 3H, OCH<sub>3</sub>), 3.85 (s, 6H, 2OCH<sub>3</sub>), 6.98 (d, *J* = 8.3 Hz, 1H, arom.CH), 7.03 (d, *J* = 7.0 Hz, 3H, arom.CH), 7.21 (s, 1H, olefinic CH), 7.26 (s, 1H, arom.CH), 7.45 (s, 2H, arom.CH), 8.29 (s, 1H, CH=N), 9.31 (s, 1H, OH), 10.01 (s, 1H, NH), 11.45 (s, 1H, NH). <sup>13</sup>C-NMR (100 MHz, DMSO-*d*<sub>6</sub>, δ ppm): 56.04 (OCH<sub>3</sub>), 56.10 (2OCH<sub>3</sub>), 56.56 (2OCH<sub>3</sub>), 60.56 (OCH<sub>3</sub>), 60.66 (OCH<sub>3</sub>), 105.98 (C2,6 trimethoxyphenyl), 107.76 (C2,6 trimethoxybenzamide), 112.37 (C2 hydroxymethoxyphenyl), 112.71 (C5 hydroxymethoxyphenyl), 120.61 (C6 hydroxymethoxyphenyl), 127.76 (C olefinic), 128.87 (C1 trimethoxyphenyl), 129.32 (C olefinic), 129.69 (C1 trimethoxybenzamide), 129.87 (C1 hydroxymethoxyphenyl), 138.58 (C4 trimethoxyphenyl), 141.04 (C4 trimethoxybenzamide), 147.35 (C=N), 148.12 (C3 hydroxymethoxyphenyl), 150.19 (C4 hydroxymethoxyphenyl), 153.07 (C3,5 trimethoxyphenyl and C3,5 trimethoxybenzamide), 162.28 (C=O trimethoxybenzamide), 165.68 (C=O hydrazide). Anal. Calcd. for C<sub>30</sub>H<sub>33</sub>N<sub>3</sub>O<sub>10</sub> (595.60): C, 60.50; H, 5.58; N, 7.06. Found: C, 60.36; H, 5.56; N, 7.09.

N-((Z)-3-((E)-2-(3,5-Dimethoxybenzylidene)hydrazinyl)-3-oxo-1-(3,4,5-trimethoxyphenyl)prop-1-en-2-yl)-3,4,5-trimethoxybenzamide (**4k**)

White powder (0.35 g, 57.12%), m.p. 214–216 °C. <sup>1</sup>H-NMR (400 MHz, DMSO-*d*<sub>6</sub>, δ ppm): 3.68 (s, 3H, OCH<sub>3</sub>), 3.68 (s, 6H, 2OCH<sub>3</sub>), 3.75 (s, 3H, OCH<sub>3</sub>), 3.80 (s, 6H, 2OCH<sub>3</sub>), 3.85 (s, 6H, 2OCH<sub>3</sub>), 6.58 (s, 1H, arom.CH), 6.86 (s, 2H, arom.CH), 7.04 (s, 2H, arom.CH), 7.19 (s, 1H, olefinic CH), 7.45 (s, 2H, arom.CH), 8.37 (s, 1H, CH=N), 10.07 (s, 1H, NH), 11.67 (s, 1H, NH). <sup>13</sup>C-NMR (100 MHz, DMSO-*d*<sub>6</sub>, δ ppm): 55.80 (2OCH<sub>3</sub>), 56.12 (2OCH<sub>3</sub>), 56.55 (2OCH<sub>3</sub>), 60.57 (OCH<sub>3</sub>), 60.65 (OCH<sub>3</sub>), 102.64 (C4 dimethoxyphenyl), 105.24 (C2,6 dimethoxyphenyl), 105.96 (C2,6 trimethoxyphenyl), 107.81 (C2,6 trimethoxybenzamide), 128.80 (C olefinic), 129.27 (C1 trimethoxyphenyl), 129.73 (C olefinic), 129.78 (C1 trimethoxybenzamide), 136.93 (C1 dimethoxyphenyl), 138.64 (C4 trimethoxyphenyl), 141.06 (C4 trimethoxybenzamide), 147.89 (C=N), 153.08 (C3,5 trimethoxyphenyl and C3,5 trimethoxybenzamide), 161.16 (C3,5 dimethoxyphenyl), 162.62 (C=O trimethoxybenzamide), 165.72 (C=O hydrazide). Anal. Calcd. for C<sub>31</sub>H<sub>35</sub>N<sub>3</sub>O<sub>10</sub> (609.62): C, 61.08; H, 5.79; N, 6.89. Found: C, 61.24; H, 5.80; N, 6.94.

3,4,5-Trimethoxy-N-((Z)-3-oxo-3-((E)-2-(3,4,5-trimethoxybenzylidene)hydrazinyl)-1-(3,4,5-trimethoxyphenyl)prop-1-en-2-yl)benzamide (**4l**)

White powder (0.32 g, 49.74%), m.p. 192–194 °C. <sup>1</sup>H-NMR (400 MHz, DMSO-*d*<sub>6</sub>, δ ppm): 3.68 (s, 9H, 3OCH<sub>3</sub>), 3.72 (s, 3H, OCH<sub>3</sub>), 3.74 (s, H, OCH<sub>3</sub>), 3.84 (s, 12H, 4OCH<sub>3</sub>), 7.01 (s, 2H, arom.CH), 7.03 (s, 2H, arom.CH), 7.44 (s, 2H, arom.CH), 8.38 (s, 1H, olefinic CH), 10.06 (s, 1H, NH), 11.63 (s, 1H, NH). <sup>13</sup>C-NMR (100 MHz, DMSO-*d*<sub>6</sub>, δ ppm): 56.12 (2OCH<sub>3</sub>), 56.41 (2OCH<sub>3</sub>), 56.55 (2OCH<sub>3</sub>), 60.57 (2OCH<sub>3</sub>), 60.65 (OCH<sub>3</sub>), 104.68 (C2,6 trimethoxyphenyl), 105.96 (C2,6 trimethoxybenzylidene), 107.79 (C2,6 trimethoxybenzamide), 128.82 (C olefinic), 129.36 (C1 trimethoxyphenyl), 129.57 (C olefinic), 129.80 (C1 trimethoxybenzylidene), 130.39 (C1 trimethoxybenzamide), 138.62 (C4 trimethoxyphenyl), 139.62 (C4 trimethoxybenzylidene), 141.04 (C4 trimethoxybenzamide), 148.07 (C=N), 153.08 (C3,5 trimethoxyphenyl and C3,5 trimethoxybenzamide), 153.66 (C3,5 trimethoxybenzylidene).

dene), 162.53 (C=O trimethoxybenzamide), 165.73 (C=O hydrazide). Anal. Calcd. for  $C_{32}H_{37}N_3O_{11}$  (639.65): C, 60.09; H, 5.83; N, 6.57. Found: C, 59.97; H, 5.86; N, 6.48.

### 3.2.2. General Procedure for the Preparation of N-((Z)-3-((E)-2-(Arylethylidene)hydrazinyl)-3-oxo-1-(3,4,5-trimethoxyphenyl)prop-1-en-2-yl)-3,4,5-trimethoxybenzamides **5a–g**

A mixture of hydrazide **1** (0.004 mol) and respective aryl halide (0.004 mol) in *n*-butanol (15 mL) was refluxed for 6–8 h. The obtained solid product was filtered off, dried and crystallized from ethanol/water (3:1) to give pure hydrazinyl compound **5a–g**.

#### 3,4,5-Trimethoxy-N-((Z)-3-oxo-3-((E)-2-(1-phenylethylidene)hydrazinyl)-1-(3,4,5-trimethoxyphenyl)prop-1-en-2-yl)benzamide (**5a**)

White powder (0.37 g, 66.19%), m.p. 260–262 °C.  $^1\text{H-NMR}$  (400 MHz,  $\text{DMSO-}d_6$ ,  $\delta$  ppm):  $^1\text{H-NMR}$  (400 MHz,  $\text{DMSO-}d_6$ ,  $\delta$  ppm): 2.31 (s, 3H,  $\text{CH}_3$ ), 3.69 (s, 9H,  $3\text{OCH}_3$ ), 3.74 (s, 3H,  $\text{OCH}_3$ ), 3.84 (s, 6H,  $2\text{OCH}_3$ ), 7.05 (s, 2H, arom.CH), 7.22 (s, 1H, olefinic CH), 7.42 (s, 5H, arom.CH), 7.84 (s, 2H, arom.CH), 10.09 (s, 1H, NH), 10.58 (s, 1H, NH).  $^{13}\text{C-NMR}$  (100 MHz,  $\text{DMSO-}d_6$ ,  $\delta$  ppm): 14.97 ( $\text{CH}_3$ ), 56.15 ( $2\text{OCH}_3$ ), 56.54 ( $2\text{OCH}_3$ ), 60.57 ( $\text{OCH}_3$ ), 60.62 ( $\text{OCH}_3$ ), 105.84 (C2,6 trimethoxyphenyl), 107.84 (C2,6 trimethoxybenzamide), 126.86 (C2,6 phenyl), 128.78 (C3,5 phenyl), 128.86 (C olefinic and C1 trimethoxyphenyl), 129.28 (C olefinic), 129.94 (C1 trimethoxybenzamide), 132.29 (C4 phenyl), 138.51 (C5 phenyl), 138.58 (C4 trimethoxyphenyl), 140.98 (C4 trimethoxybenzamide), 149.84 (C=N), 153.06 (C3,5 trimethoxyphenyl), 153.09 (C3,5 trimethoxybenzamide), 162.50 (C=O trimethoxybenzamide), 165.93 (C=O hydrazide). Anal. Calcd. for  $C_{30}H_{33}N_3O_8$  (563.60): C, 63.93; H, 5.90; N, 7.46. Found: C, 64.18; H, 6.08; N, 7.57.

#### N-((Z)-3-((E)-2-(1-(4-Chlorophenyl)ethylidene)hydrazinyl)-3-oxo-1-(3,4,5-trimethoxyphenyl)prop-1-en-2-yl)-3,4,5-trimethoxybenzamide (**5b**)

White powder (0.36 g, 59.73%), m.p. 249–251 °C.  $^1\text{H-NMR}$  (400 MHz,  $\text{DMSO-}d_6$ ,  $\delta$  ppm): 2.30 (s, 3H,  $\text{CH}_3$ ), 3.69 (s, 6H,  $2\text{OCH}_3$ ), 3.69 (s, 3H,  $\text{OCH}_3$ ), 3.74 (s, 3H,  $\text{OCH}_3$ ), 3.83 (s, 6H,  $2\text{OCH}_3$ ), 7.05 (s, 2H, arom.CH), 7.19 (s, 1H, olefinic CH), 7.41 (s, 2H, arom.CH), 7.50 (s, 2H, arom.CH), 7.85 (s, 2H, arom.CH), 10.10 (s, 1H, NH), 10.63 (s, 1H, NH).  $^{13}\text{C-NMR}$  (100 MHz,  $\text{DMSO-}d_6$ ,  $\delta$  ppm): 14.87 ( $\text{CH}_3$ ), 56.16 ( $2\text{OCH}_3$ ), 56.54 ( $2\text{OCH}_3$ ), 60.57 ( $\text{OCH}_3$ ), 60.62 ( $\text{OCH}_3$ ), 105.83 (C2,6 trimethoxyphenyl), 107.85 (C2,6 trimethoxybenzamide), 128.60 (C2,6 chlorophenyl), 128.83 (C3,5 chlorophenyl), 129.34 (C olefinic), 129.75 (C1 trimethoxyphenyl), 129.91 (C olefinic), 130.72 (C1 trimethoxybenzamide), 134.53 (C1 chlorophenyl), 137.34 (C4 chlorophenyl), 138.60 (C4 trimethoxyphenyl), 140.98 (C4 trimethoxybenzamide), 148.64 (C=N), 153.07 (C3,5 trimethoxyphenyl), 153.09 (C3,5 trimethoxybenzamide), 162.59 (C=O trimethoxybenzamide), 165.95 (C=O hydrazide). Anal. Calcd. for  $C_{30}H_{32}ClN_3O_8$  (598.04): C, 60.25; H, 5.39; N, 7.03. Found: C, 59.98; H, 5.17; N, 7.22.

#### N-((Z)-3-((E)-2-(1-(4-Bromophenyl)ethylidene)hydrazinyl)-3-oxo-1-(3,4,5-trimethoxyphenyl)prop-1-en-2-yl)-3,4,5-trimethoxybenzamide (**5c**)

White powder (0.39 g, 61.10%), m.p. 244–246 °C.  $^1\text{H-NMR}$  (400 MHz,  $\text{DMSO-}d_6$ ,  $\delta$  ppm): 2.29 (s, 3H,  $\text{CH}_3$ ), 3.69 (s, 3H,  $\text{OCH}_3$ ), 3.69 (s, 6H,  $2\text{OCH}_3$ ), 3.74 (s, 3H,  $\text{OCH}_3$ ), 3.83 (s, 6H,  $2\text{OCH}_3$ ), 7.05 (s, 2H, arom.CH), 7.19 (s, 1H, olefinic CH), 7.41 (s, 2H, arom.CH), 7.64 (s, 2H, arom.CH), 7.78 (s, 2H, arom.CH), 10.10 (s, 1H, NH), 10.63 (s, 1H, NH).  $^{13}\text{C-NMR}$  (100 MHz,  $\text{DMSO-}d_6$ ,  $\delta$  ppm): 14.82 ( $\text{CH}_3$ ), 56.16 ( $2\text{OCH}_3$ ), 56.54 ( $2\text{OCH}_3$ ), 60.58 ( $\text{OCH}_3$ ), 60.62 ( $\text{OCH}_3$ ), 105.83 (C2,6 trimethoxyphenyl), 107.86 (C2,6 trimethoxybenzamide), 125.78 (C4 bromophenyl), 128.82 (C2,6 bromophenyl), 128.87 (C3,5 bromophenyl), 129.84 (C olefinic), 129.90 (C1 trimethoxyphenyl), 131.09 (C olefinic), 131.74 (C1 trimethoxybenzamide), 137.70 (C1 bromophenyl), 138.60 (C4 trimethoxyphenyl), 140.99 (C4 trimethoxybenzamide), 145.56 (C=N), 153.07 (C3,5 trimethoxyphenyl), 153.09 (C3,5 trimethoxybenzamide), 161.06 (C=O

trimethoxybenzamide), 165.89 (C=O hydrazide). Anal. Calcd. for  $C_{30}H_{32}BrN_3O_8$  (642.49): C, 56.08; H, 5.02; N, 6.54. Found: C, 55.86; H, 4.92; N, 6.79.

N-((Z)-3-((E)-2-(1-(4-Hydroxyphenyl)ethylidene)hydrazinyl)-3-oxo-1-(3,4,5-trimethoxyphenyl)prop-1-en-2-yl)-3,4,5-trimethoxybenzamide (**5d**)

White powder (0.32 g, 55.42%), m.p. 258–260 °C.  $^1H$ -NMR (400 MHz, DMSO- $d_6$ ,  $\delta$  ppm): 2.23 (s, 3H, CH<sub>3</sub>), 3.68 (s, 9H, 3OCH<sub>3</sub>), 3.74 (s, 3H, OCH<sub>3</sub>), 3.84 (s, 6H, 2OCH<sub>3</sub>), 6.77–6.88 (m, 2H, arom.CH), 7.03 (s, 2H, arom.CH), 7.22 (s, 1H, olefinic CH), 7.42 (s, 2H, arom.CH), 7.70 (d,  $J$  = 6.2 Hz, 2H, arom.CH), 9.80 (s, 1H, OH), 10.05 (s, 1H, NH), 10.43 (s, 1H, NH).  $^{13}C$ -NMR (100 MHz, DMSO- $d_6$ ,  $\delta$  ppm): 14.85 (CH<sub>3</sub>), 56.13 (2OCH<sub>3</sub>), 56.54 (2OCH<sub>3</sub>), 60.56 (OCH<sub>3</sub>), 60.62 (OCH<sub>3</sub>), 105.86 (C2,6 trimethoxyphenyl), 107.79 (C2,6 trimethoxybenzamide), 115.51 (C3,5 hydroxyphenyl), 115.60 (C1 hydroxyphenyl), 128.50 (C2,6 hydroxyphenyl), 128.94 (C olefinic), 129.28 (C1 trimethoxyphenyl), 129.96 (C olefinic), 131.16 (C1 trimethoxybenzamide), 138.54 (C4 trimethoxyphenyl), 140.96 (C4 trimethoxybenzamide), 146.58 (C=N), 153.05 (C3,5 trimethoxyphenyl and C3,5 trimethoxybenzamide), 159.38 (C4 hydroxyphenyl), 162.12 (C=O trimethoxybenzamide), 166.02 (C=O hydrazide). Anal. Calcd. for  $C_{30}H_{33}N_3O_9$  (579.60): C, 62.17; H, 5.74; N, 7.25. Found: C, 62.31; H, 5.96; N, 6.99.

3,4,5-Trimethoxy-N-((Z)-3-((E)-2-(1-(4-methoxyphenyl)ethylidene)hydrazinyl)-3-oxo-1-(3,4,5-trimethoxyphenyl)prop-1-en-2-yl)benzamide (**5e**)

White powder (0.37 g, 62.58%), m.p. 241–243 °C.  $^1H$ -NMR (400 MHz, DMSO- $d_6$ ,  $\delta$  ppm): 2.26 (s, 3H, CH<sub>3</sub>), 3.68 (s, 9H, 3OCH<sub>3</sub>), 3.74 (s, 3H, OCH<sub>3</sub>), 3.81 (s, 3H, OCH<sub>3</sub>), 3.84 (s, 6H, 2OCH<sub>3</sub>), 6.91–7.09 (m, 4H, arom.CH), 7.22 (s, 1H, olefinic CH), 7.42 (s, 2H, arom.CH), 7.83 (d,  $J$  = 10.4 Hz, 2H, arom.CH), 10.06 (s, 1H, OH), 10.49 (s, 1H, NH).  $^{13}C$ -NMR (100 MHz, DMSO- $d_6$ ,  $\delta$  ppm): 14.95 (CH<sub>3</sub>), 55.71 (OCH<sub>3</sub>), 56.14 (2OCH<sub>3</sub>), 56.54 (2OCH<sub>3</sub>), 60.57 (OCH<sub>3</sub>), 60.62 (OCH<sub>3</sub>), 105.86 (C2,6 trimethoxyphenyl), 107.81 (C2,6 trimethoxybenzamide), 114.13 (C3,5 methoxyphenyl), 127.95 (C2,6 methoxyphenyl), 128.40 (C olefinic), 128.53 (C1 trimethoxyphenyl), 128.92 (C olefinic), 129.96 (C1 trimethoxybenzamide), 130.86 (C1 methoxyphenyl), 138.55 (C4 trimethoxyphenyl), 140.96 (C4 trimethoxybenzamide), 146.20 (C=N), 153.06 (C3,5 trimethoxyphenyl), 153.08 (C3,5 trimethoxybenzamide), 158.92 (C4 methoxyphenyl), 162.33 (C=O trimethoxybenzamide), 169.79 (C=O hydrazide). Anal. Calcd. for  $C_{31}H_{35}N_3O_9$  (593.62): C, 62.72; H, 5.94; N, 7.08. Found: C, 62.79; H, 5.97; N, 7.02.

N-((Z)-3-((E)-2-(1-(3,4-Dimethoxyphenyl)ethylidene)hydrazinyl)-3-oxo-1-(3,4,5-trimethoxyphenyl)prop-1-en-2-yl)-3,4,5-trimethoxybenzamide (**5f**)

White powder (0.44 g, 71.06%), m.p. 234–236 °C.  $^1H$ -NMR (400 MHz, DMSO- $d_6$ ,  $\delta$  ppm): 2.28 (s, 3H, CH<sub>3</sub>), 3.68 (s, 9H, 3OCH<sub>3</sub>), 3.74 (s, 3H, OCH<sub>3</sub>), 3.81 (s, 3H, OCH<sub>3</sub>), 3.84 (s, 9H, 3OCH<sub>3</sub>), 7.03 (s, 2H, arom.CH), 7.21 (s, 1H, olefinic CH), 7.32–7.54 (m, 4H, arom.CH), 7.92 (d,  $J$  = 7.4 Hz, 1H, arom.CH), 10.07 (s, 1H, NH), 10.53 (s, 1H, NH).  $^{13}C$ -NMR (100 MHz, DMSO- $d_6$ ,  $\delta$  ppm): 15.04 (CH<sub>3</sub>), 56.00 (2OCH<sub>3</sub>), 56.15 (2OCH<sub>3</sub>), 56.54 (2OCH<sub>3</sub>), 60.57 (OCH<sub>3</sub>), 60.63 (OCH<sub>3</sub>), 105.87 (C2,6 trimethoxyphenyl), 107.79 (C2,6 trimethoxybenzamide), 109.75 (C5 dimethoxyphenyl), 111.54 (C2 dimethoxyphenyl), 120.35 (C6 dimethoxyphenyl), 126.89 (C1 dimethoxyphenyl), 128.93 (C olefinic), 129.37 (C1 trimethoxyphenyl), 129.97 (C olefinic), 130.26 (C1 trimethoxybenzamide), 131.02 (C1 trimethoxyphenyl), 138.55 (C4 trimethoxyphenyl), 140.96 (C4 trimethoxybenzamide), 148.90 (C=N), 150.81 (C3 dimethoxyphenyl), 153.06 (C3,5 trimethoxyphenyl), 153.07 (C3,5 trimethoxybenzamide), 156.90 (C4 dimethoxyphenyl), 162.31 (C=O trimethoxybenzamide), 166.02 (C=O hydrazide). Anal. Calcd. for  $C_{32}H_{37}N_3O_{10}$  (623.65): C, 61.63; H, 5.98; N, 6.74. Found: C, 61.74; H, 6.11; N, 6.62.



3,4,5-Trimethoxy-N-((Z)-3-oxo-1-(3,4,5-trimethoxyphenyl)-3-((E)-2-(1-(3,4,5-trimethoxyphenyl)ethylidene)hydrazinyl)prop-1-en-2-yl)benzamide (**5g**)

White powder (0.36 g, 55.19%), m.p. 211–213 °C. <sup>1</sup>H-NMR (400 MHz, DMSO-*d*<sub>6</sub>, δ ppm): 2.31 (s, 3H, CH<sub>3</sub>), 3.69 (s, 12H, 4OCH<sub>3</sub>), 3.74 (s, 3H, OCH<sub>3</sub>), 3.84 (s, 12H, 4OCH<sub>3</sub>), 7.04 (s, 2H, arom.CH), 7.13 (s, 2H, arom.CH), 7.20 (s, 1H, olefinic CH), 7.42 (s, 2H, arom.CH), 10.08 (s, 1H, NH), 10.60 (s, 1H, NH). <sup>13</sup>C-NMR (100 MHz, DMSO-*d*<sub>6</sub>, δ ppm): 15.31 (CH<sub>3</sub>), 56.16 (2OCH<sub>3</sub>), 56.30 (OCH<sub>3</sub>), 56.42 (OCH<sub>3</sub>), 56.53 (2OCH<sub>3</sub>), 60.58 (2OCH<sub>3</sub>), 60.62 (OCH<sub>3</sub>), 104.54 (C2,6 trimethoxyphenyl), 105.86 (C2,6 trimethoxyphenylethylidene), 107.80 (C2,6 trimethoxyphenyl), 123.94 (C1 trimethoxyphenylethylidene), 128.90 (C olefinic), 129.29 (C1 trimethoxyphenyl), 129.94 (C olefinic), 130.26 (C1 trimethoxybenzamide), 136.66 (C4 trimethoxyphenylethylidene), 138.55 (C4 trimethoxyphenyl), 140.97 (C4 trimethoxybenzamide), 145.37 (C=N), 153.07 (C3,5 trimethoxyphenylethylidene), 153.08 (C3,5 trimethoxyphenyl and C3,5 trimethoxybenzamide), 165.92 (C=O trimethoxybenzamide), 170.63 (C=O hydrazide). Anal. Calcd. for C<sub>33</sub>H<sub>39</sub>N<sub>3</sub>O<sub>11</sub> (653.68): C, 60.63; H, 6.01; N, 6.43. Found: C, 60.47; H, 5.86; N, 6.61.

### 3.3. Biological Assays

#### 3.3.1. Cytotoxic Activity against MDA-MB-231 Cell Line

Cytotoxic activity of the prepared schiff bases against MDA-MB-231 breast cell Line was determined according previously reported methods [45]. (See Supplementary Materials—Appendix SB).

#### 3.3.2. Tubulin Inhibition Assays

Compound **4h** was evaluated for their Tubulin inhibitory activity according to manufacturer's instructions [38].

#### 3.3.3. Cell Cycle Analysis of Compound 4h

See Supplementary Materials—Appendix SB.

#### 3.3.4. Annexin V FITC/PI Staining Assay for Compound 4h

See Supplementary Materials—Appendix SB.

#### 3.3.5. Mitochondrial Membrane Potential

See Supplementary Materials—Appendix SB.

#### 3.3.6. ELISA Measurements of p53, Bax and Bcl-2

See Supplementary Materials—Appendix SB.

#### 3.3.7. Molecular Docking Study

See Supplementary Materials—Appendix SB.

### 3.4. Fabrication of Compound 4h Loaded NLCs

Briefly, the organic phase composed of lipid either Precirol ATO-5 or Geleol in either 2% or 6% along with Capryol 90 were dispersed in THF along with **4h** which was dripped slowly to an aqueous phase composing either 1 or 2% of a surfactant (Cremophor RH40) under stirring. The attained primary O/W emulsion was introduced to ultrasonication using a probe sonicator for 10 min at 60% amplitude (Model 275 T Crest Ultrasonics Corp., Trenton, NJ, USA). Finally, the resulting emulsion was kept under continuous stirring (MS-300HS, Misung Scientific Co., Korea) to permit the complete evaporation of the organic solvent and the precipitation of **4h**-NLCs [39].

#### 4. Conclusions

**Finally:** new Schiff base-based TMP compounds were synthesized and evaluated for their cytotoxic activity against the breast MDA-MB-231 cell line and the normal breast MCF-10A to conclude this research. The tested Schiff bases revealed good activity over the MDA-MB-231 cell line, especially compounds **4h**, **4j** and **5d** with  $IC_{50}$  values  $1.27 \pm 0.18 \mu\text{M}$ ,  $2.84 \pm 0.18 \mu\text{M}$  and  $1.98 \pm 0.19 \mu\text{M}$ , respectively, compared to CA-4 ( $IC_{50} = 0.54 \pm 0.04$ ). The cytotoxic activity of Schiff base **4h** is correlated to tubulin polymerization inhibitory activity as revealed by immunofluorescence analysis and  $\beta$ -tubulin polymerization inhibition percentage on MDA-MB-231 cells (78.14% polymerization inhibition at  $1.27 \mu\text{M}$ ). In addition, compound **4h** caused cell cycle arrest at the G2/M phase (fivefold more than control MDA-MB-231 cells) and cellular apoptosis as ascertained by an increase in the percentage of the pre-G1 phase by almost 19-fold compared with negative control cells and Annexin V FITC/PI staining assay. Moreover, compound **4h** was found to be an apoptotic inducer via a decrease in the level of MMP and Bcl-2 by 3- and 8-fold, respectively, compared to negative control cells and an increase in the level of p53 and Bax by 11- and 5-fold, respectively, compared to the negative control cells. Additionally, the most potent compound **4h** was lodged on nanostructured lipid carriers (NLCs). Eight formulae resulted from  $2^3$  full factorial design which was conducted to govern the influence of the fabrication variables on the in vitro characters of the casted NLCs. Based on the outcomes of the experimental design and factorial analysis, F3 was picked as the optimum formula exhibiting a dominant desirability value of 0.805, EE%  $95.6 \pm 2.4$ , PS  $222.4 \pm 18.7$ , PDI  $0.23 \pm 0.05$  and ZP  $-39.2 \pm 3.9$  Mv. Moreover, F3 exhibited an improved release and solubility profile over that of the drug suspension. In the comparative cytotoxic activity, F3 was capable of diminishing the  $IC_{50}$  by around 2.15 times for pure **4h**, while nearly close to the  $IC_{50}$  of the reference drug. Thus, NLCs could be a potential platform for boosted antitumor activity of compound **4h** against MDA-MB-231 cancer cells.

**Supplementary Materials:** The following supporting information can be downloaded at: <https://www.mdpi.com/article/10.3390/ph15060679/s1>, Figure S1:  $^1\text{H-NMR}$  spectrum of compound **2**, Figure S2:  $^{13}\text{C-NMR}$  spectrum of compound **2**, Figure S3:  $^1\text{H-NMR}$  spectrum of compound **3**, Figure S4:  $^{13}\text{C-NMR}$  spectrum of compound **3**, Figure S5:  $^1\text{H-NMR}$  spectrum of compound **4a**, Figure S6:  $^{13}\text{C-NMR}$  spectrum of compound **4a**, Figure S7:  $^1\text{H-NMR}$  spectrum of compound **4b**, Figure S8:  $^{13}\text{C-NMR}$  spectrum of compound **4b**, Figure S9:  $^1\text{H-NMR}$  spectrum of compound **4c**, Figure S10:  $^{13}\text{C-NMR}$  spectrum of compound **4c**, Figure S11:  $^1\text{H-NMR}$  spectrum of compound **4d**, Figure S12:  $^{13}\text{C-NMR}$  spectrum of compound **4d**, Figure S13:  $^1\text{H-NMR}$  spectrum of compound **4e**, Figure S14:  $^{13}\text{C-NMR}$  spectrum of compound **4e**, Figure S15:  $^1\text{H-NMR}$  spectrum of compound **4f**, Figure S16:  $^{13}\text{C-NMR}$  spectrum of compound **4f**, Figure S17:  $^1\text{H-NMR}$  spectrum of compound **4g**, Figure S18:  $^{13}\text{C-NMR}$  spectrum of compound **4g**, Figure S19:  $^1\text{H-NMR}$  spectrum of compound **4h**, Figure S20:  $^{13}\text{C-NMR}$  spectrum of compound **4h**, Figure S21:  $^1\text{H-NMR}$  spectrum of compound **4i**, Figure S22:  $^{13}\text{C-NMR}$  spectrum of compound **4i**, Figure S23:  $^1\text{H-NMR}$  spectrum of compound **4j**, Figure S24:  $^{13}\text{C-NMR}$  spectrum of compound **4j**, Figure S25:  $^1\text{H-NMR}$  spectrum of compound **4k**, Figure S26:  $^{13}\text{C-NMR}$  spectrum of compound **4k**, Figure S27:  $^1\text{H-NMR}$  spectrum of compound **4l**, Figure S28:  $^{13}\text{C-NMR}$  spectrum of compound **4l**, Figure S29:  $^1\text{H-NMR}$  spectrum of compound **5a**, Figure S30:  $^{13}\text{C-NMR}$  spectrum of compound **5a**, Figure S31:  $^1\text{H-NMR}$  spectrum of compound **5b**, Figure S32:  $^{13}\text{C-NMR}$  spectrum of compound **5b**, Figure S33:  $^1\text{H-NMR}$  spectrum of compound **5c**, Figure S34:  $^{13}\text{C-NMR}$  spectrum of compound **5c**, Figure S35:  $^1\text{H-NMR}$  spectrum of compound **5d**, Figure S36:  $^{13}\text{C-NMR}$  spectrum of compound **5d**, Figure S37:  $^1\text{H-NMR}$  spectrum of compound **5e**, Figure S38:  $^{13}\text{C-NMR}$  spectrum of compound **5e**, Figure S39:  $^1\text{H-NMR}$  spectrum of compound **5f**, Figure S40:  $^{13}\text{C-NMR}$  spectrum of compound **5f**, Figure S41:  $^1\text{H-NMR}$  spectrum of compound **5g**, Figure S42:  $^{13}\text{C-NMR}$  spectrum of compound **5g**, Appendix SA and Appendix SB.

**Author Contributions:** Conceptualization, M.Y.Z., I.Z. and S.N.A.B.; methodology, S.N.A.B., M.Y.Z., M.U.M., R.E.B. and I.Z.; data curation, M.Y.Z., M.A.E., A.K.H., A.H.A.A. and I.Z.; software, S.N.A.B., M.Y.Z., R.E.B., A.K.H. and I.Z.; resources, S.N.A.B., M.Y.Z., M.U.M., N.A., M.A.E. and I.Z.; supervision, M.Y.Z., I.Z. and S.N.A.B.; funding acquisition, S.N.A.B., M.U.M., N.A. and M.A.E. original draft preparation, M.Y.Z., R.E.B. and I.Z.; Writing, review, and editing, all authors. All authors have read and agreed to the published version of the manuscript.

**Funding:** The authors' work was supported through grant number "375213500" from the Deputyship for Research and Innovation, Ministry of Education in Saudi Arabia.

**Institutional Review Board Statement:** Not applicable.

**Informed Consent Statement:** Not applicable.

**Data Availability Statement:** Data is contained within the article and supplementary material.

**Acknowledgments:** The authors extend their appreciation to the Deputyship for Research and Innovation, Ministry of Education in Saudi Arabia, and the central laboratory at Jouf University for supporting this study.

**Conflicts of Interest:** The authors declare no conflict of interest.

## References

1. Mukhtar, E.; Adhami, V.M.; Mukhtar, H. Targeting Microtubules by Natural Agents for Cancer Therapy. *Mol. Cancer Ther.* **2014**, *13*, 275–284. [\[CrossRef\]](#)
2. Eli, S.; Castagna, R.; Mapelli, M.; Parisini, E. Recent Approaches to the Identification of Novel Microtubule-Targeting Agents. *Front. Mol. Biosci.* **2022**, *9*, 841777. [\[CrossRef\]](#)
3. Jordan, M.A.; Wilson, L. Microtubules as a target for anticancer drugs. *Nat. Cancer* **2004**, *4*, 253–265.
4. Chatterjee, S.; Som, S.; Varshney, N.; Satyadev, P.V.S.; Sanyal, K.; Paul, R. Mechanics of microtubule organizing center clustering and spindle positioning in budding yeast *Cryptococcus neoformans*. *Phys. Rev. E* **2021**, *104*, 034402. [\[CrossRef\]](#)
5. Li, G.; Hu, X.; Wu, X.; Zhang, Y. Microtubule-Targeted Self-Assembly Triggers Prometaphase–Metaphase Oscillations Suppressing Tumor Growth. *Nano Lett.* **2021**, *21*, 3052–3059. [\[CrossRef\]](#)
6. Janke, C.; Magiera, M.M. The tubulin code and its role in controlling microtubule properties and functions. *Nat. Rev. Mol. Cell Biol.* **2020**, *21*, 307–326.
7. Barreca, M.; Stathis, A.; Barraja, P.; Bertoni, F. An overview on anti-tubulin agents for the treatment of lymphoma patients. *Pharmacol. Ther.* **2020**, *211*, 107552.
8. Qi, F.; Zhou, J.; Liu, M. Microtubule-interfering agents, spindle defects, and interkinetochore tension. *J. Cell. Physiol.* **2020**, *235*, 26–30. [\[CrossRef\]](#)
9. Arnst, K.E.; Banerjee, S.; Chen, H.; Deng, S.; Hwang, D.-J.; Li, W.; Miller, D.D. Current advances of tubulin inhibitors as dual acting small molecules for cancer therapy. *Med. Res. Rev.* **2019**, *39*, 1398–1426. [\[CrossRef\]](#)
10. Li, L.; Jiang, S.; Li, X.; Liu, Y.; Su, J.; Chen, J. Recent advances in trimethoxyphenyl (TMP) based tubulin inhibitors targeting the colchicine binding site. *Eur. J. Med. Chem.* **2018**, *151*, 482–494. [\[CrossRef\]](#)
11. Sun, K.; Sun, Z.; Zhao, F.; Shan, G.; Meng, Q. Recent advances in research of colchicine binding site inhibitors and their interaction modes with tubulin. *Future Med. Chem.* **2021**, *13*, 839–858. [\[CrossRef\]](#)
12. Duan, Y.; Liu, W.; Tian, L.; Mao, Y.; Song, C. Targeting tubulin-colchicine site for cancer therapy: Inhibitors, antibody-drug conjugates and degradation agents. *Curr. Top. Med. Chem.* **2019**, *19*, 1289–1304.
13. Kerr, D.J.; Hamel, E.; Jung, M.K.; Flynn, B.L. The concise synthesis of chalcone, indanone and indenone analogues of combretastatin A4. *Bioorg. Med. Chem.* **2007**, *15*, 3290–3298. [\[CrossRef\]](#)
14. Shawky, A.M.; Ibrahim, N.A.; Abdalla, A.N.; Abourehab, M.A.S.; Gouda, A.M. Novel pyrrolizines bearing 3,4,5-trimethoxyphenyl moiety: Design, synthesis, molecular docking, and biological evaluation as potential multi-target cytotoxic agents. *J. Enzym. Inhib. Med. Chem.* **2021**, *36*, 1312–1332. [\[CrossRef\]](#)
15. Ansari, M.; Shokrzadeh, M.; Karima, S.; Rajaei, S.; Fallah, M.; Ghassemi-Barghi, N.; Ghasemian, M.; Emami, S. New thiazole-2(3H)-thiones containing 4-(3,4,5-trimethoxyphenyl) moiety as anticancer agents. *Eur. J. Med. Chem.* **2020**, *185*, 111784. [\[CrossRef\]](#)
16. Hamze, A.; Alami, M.; Provot, O. Developments of isoCombretastatin A-4 derivatives as highly cytotoxic agents. *Eur. J. Med. Chem.* **2020**, *190*, 112110. [\[CrossRef\]](#)
17. Naaz, F.; Haider, M.R.; Shafi, S.; Yar, M.S. Anti-tubulin agents of natural origin: Targeting taxol, vinca, and colchicine binding domains. *Eur. J. Med. Chem.* **2019**, *171*, 310–331.
18. Gaspari, R.; Prota, A.E.; Bargsten, K.; Cavalli, A.; Steinmetz, M.O. Structural Basis of cis- and trans-Combretastatin Binding to Tubulin. *Chem* **2017**, *2*, 102–113. [\[CrossRef\]](#)
19. Pettit, G.R.; Toki, B.; Herald, D.L.; Verdier-Pinard, P.; Boyd, M.R.; Hamel, E.; Pettit, R.K. Antineoplastic Agents. 379. Synthesis of Phenstatin Phosphate1a. *J. Med. Chem.* **1998**, *41*, 1688–1695. [\[CrossRef\]](#)

20. Fortin, S.; Wei, L.; Moreau, E.; Lacroix, J.; Côté, M.-F.; Petitclerc, É.; Kotra, L.P.; Gaudreault, R.C. Substituted phenyl 4-(2-oxoimidazolidin-1-yl)benzenesulfonamides as antimetabolites. Antiproliferative, antiangiogenic and antitumoral activity, and quantitative structure-activity relationships. *Eur. J. Med. Chem.* **2011**, *46*, 5327–5342. [[CrossRef](#)]
21. Yan, J.; Chen, J.; Zhang, S.; Hu, J.; Huang, L.; Li, X. Synthesis, Evaluation, and Mechanism Study of Novel Indole-Chalcone Derivatives Exerting Effective Antitumor Activity through Microtubule Destabilization In Vitro and In Vivo. *J. Med. Chem.* **2016**, *59*, 5264–5283. [[CrossRef](#)]
22. Maklad, R.M.; AbdelHafez, E.-S.M.N.; Abdelhamid, D.; Aly, O.M. Tubulin inhibitors: Discovery of a new scaffold targeting extra-binding residues within the colchicine site through anchoring substituents properly adapted to their pocket by a semi-flexible linker. *Bioorg. Chem.* **2020**, *99*, 103767. [[CrossRef](#)]
23. Uddin, N.; Rashid, F.; Ali, S.; Tirmizi, S.A.; Ahmad, I.; Zaib, S.; Zubair, M.; Diaconescu, P.L.; Tahir, M.N.; Iqbal, J.; et al. Synthesis, characterization, and anticancer activity of Schiff bases. *J. Biomol. Struct. Dyn.* **2020**, *38*, 3246–3259. [[CrossRef](#)]
24. Cordeiro, R.; Kachroo, M. Synthesis and biological evaluation of anti-tubercular activity of Schiff bases of 2-Amino thiazoles. *Bioorg. Med. Chem. Lett.* **2020**, *30*, 127655. [[CrossRef](#)]
25. Singh, G.; Kalra, P.; Singh, A.; Sharma, G.; Espinosa-Ruiz, C.; Esteban, M.A. A quick microwave preparation of isatin hydrazone schiff base conjugated organosilicon compounds: Exploration of their antibacterial, antifungal, and antioxidative potentials. *J. Organomet. Chem.* **2021**, *953*, 122051. [[CrossRef](#)]
26. Sundaree, S.; Vaddula, B.R.; Tantak, M.P.; Khandagale, S.B.; Shi, C.; Shah, K.; Kumar, D. Synthesis and anticancer activity study of indolyl hydrazide-hydrazones. *Med. Chem. Res.* **2016**, *25*, 941–950. [[CrossRef](#)]
27. Acharya, S.; Maji, M.; Chakraborty, M.P.; Bhattacharya, I.; Das, R.; Gupta, A.; Mukherjee, A. Disruption of the Microtubule Network and Inhibition of VEGFR2 Phosphorylation by Cytotoxic N,O-Coordinated Pt(II) and Ru(II) Complexes of Trimethoxy Aniline-Based Schiff Bases. *Inorg. Chem.* **2021**, *60*, 3418–3430. [[CrossRef](#)]
28. Nasr, T.; Bondock, S.; Youns, M. Anticancer activity of new coumarin substituted hydrazide-hydrazone derivatives. *Eur. J. Med. Chem.* **2014**, *76*, 539–548. [[CrossRef](#)]
29. Zaki, I.; El-ata, S.A.A.; Fayad, E.; Ali, O.A.A.; Almaaty, A.H.A.; Saad, A.S. Evaluation of Synthetic 2,4-Disubstituted-benzo[g]quinoxaline Derivatives as Potential Anticancer Agents. *Pharmaceuticals* **2021**, *14*, 853. [[CrossRef](#)]
30. Almaaty, A.H.A.; Toson, E.E.M.; El-Sayed, E.-S.H.; Tantawy, M.A.M.; Fayad, E.; Ali, O.A.A.; Zaki, I. 5-Aryl-1-Arylideneamino-1H-Imidazole-2(3H)-Thiones: Synthesis and In Vitro Anticancer Evaluation. *Molecules* **2021**, *26*, 1706. [[CrossRef](#)]
31. Zaki, I.; Abdelhameid, M.K.; El-Deen, I.M.; Wahab, A.H.A.A.; Ashmawy, A.M.; Mohamed, K.O. Design, synthesis and screening of 1, 2, 4-triazinone derivatives as potential antitumor agents with apoptosis inducing activity on MCF-7 breast cancer cell line. *Eur. J. Med. Chem.* **2018**, *156*, 563–579. [[CrossRef](#)]
32. Zaki, I.; Masoud, R.E.; Hamoud, M.M.S.; Ali, O.A.A.; Abualnaja, M.; Fayad, E.; Almaaty, A.H.A.; Elnaghia, L.K. Design, synthesis and cytotoxicity screening of new synthesized pyrimidine-5-carbonitrile derivatives showing marked apoptotic effect. *J. Mol. Struct.* **2022**, *1259*, 132749. [[CrossRef](#)]
33. Tang, S.; Zhou, Z.; Jiang, Z.; Zhu, W.; Qiao, D. Indole-Based Tubulin Inhibitors: Binding Modes and SARs Investigations. *Molecules* **2022**, *27*, 1587. [[CrossRef](#)]
34. Liao, W.-L.; Lin, J.-Y.; Shieh, J.-C.; Yeh, H.-F.; Hsieh, Y.-H.; Cheng, Y.-C.; Lee, H.-J.; Shen, C.-Y.; Cheng, C.-W. Induction of G2/M Phase Arrest by Diosgenin via Activation of Chk1 Kinase and Cdc25C Regulatory Pathways to Promote Apoptosis in Human Breast Cancer Cells. *Int. J. Mol. Sci.* **2020**, *21*, 172. [[CrossRef](#)]
35. Li, M. The role of P53 up-regulated modulator of apoptosis (PUMA) in ovarian development, cardiovascular and neurodegenerative diseases. *Apoptosis* **2021**, *26*, 235–247. [[CrossRef](#)]
36. Das, S.; Ng, W.K.; Tan, R.B.H. Are nanostructured lipid carriers (NLCs) better than solid lipid nanoparticles (SLNs): Development, characterizations and comparative evaluations of clotrimazole-loaded SLNs and NLCs? *Eur. J. Pharm. Sci.* **2012**, *47*, 139–151. [[CrossRef](#)]
37. Kaur, S.; Nautyal, U.; Singh, R.; Singh, S.; Devi, A. Nanostructure lipid carrier (NLC): The new generation of lipid nanoparticles. *Asian Pac. J. Health Sci.* **2015**, *2*, 76–93. [[CrossRef](#)]
38. Zaki, I.; Abou-Elkhair, R.A.I.; Almaaty, A.H.A.; Ali, O.A.A.; Fayad, E.; Gaafar, A.G.A.; Zakaria, M.Y. Design and Synthesis of Newly Synthesized Acrylamide Derivatives as Potential Chemotherapeutic Agents against MCF-7 Breast Cancer Cell Line Lodged on PEGylated Bilosomal Nano-Vesicles for Improving Cytotoxic Activity. *Pharmaceuticals* **2021**, *14*, 1021. [[CrossRef](#)]
39. El-Halim, S.M.A.; Abdelbary, G.A.; Amin, M.M.; Zakaria, M.Y.; Shamsel-Din, H.A.; Ibrahim, A.B. Stabilized oral nanostructured lipid carriers of Adefovir Dipivoxil as a potential liver targeting: Estimation of liver function panel and uptake following intravenous injection of radioiodinated indicator. *DARU J. Pharm. Sci.* **2020**, *28*, 517–532. [[CrossRef](#)]
40. Aburahma, M.H.; Badr-Eldin, S.M. Compritol 888 ATO: A multifunctional lipid excipient in drug delivery systems and nanopharmaceuticals. *Expert Opin. Drug Deliv.* **2014**, *11*, 1865–1883. [[CrossRef](#)]
41. Poonia, N.; Kharb, R.; Lather, V.; Pandita, D. Nanostructured lipid carriers: Versatile oral delivery vehicle. *Future Sci.* **2016**, *2*, FSO135. [[CrossRef](#)]
42. Sznitowska, M.; Wolska, E.; Baranska, H.; Cal, K.; Pietkiewicz, J. The effect of a lipid composition and a surfactant on the characteristics of the solid lipid microspheres and nanospheres (SLM and SLN). *Eur. J. Pharm. Biopharm.* **2017**, *110*, 24–30. [[CrossRef](#)]

43. El-Zaafarany, G.M.; Soliman, M.E.; Mansour, S.; Awad, G.A.S. Identifying lipidic emulsomes for improved oxcarbazepine brain targeting: In vitro and rat in vivo studies. *Int. J. Pharm.* **2016**, *503*, 127–140. [[CrossRef](#)]
44. Zakaria, M.Y.; Fayad, E.; Althobaiti, F.; Zaki, I.; Almaaty, A.H.A. Statistical optimization of bile salt deployed nanovesicles as a potential platform for oral delivery of piperine: Accentuated antiviral and anti-inflammatory activity in MERS-CoV challenged mice. *Drug Deliv.* **2021**, *28*, 1150–1165. [[CrossRef](#)]
45. Abdelhaleem, E.F.; Abdelhameid, M.K.; Kassab, A.E.; Kandeel, M.M. Design and synthesis of thienopyrimidine urea derivatives with potential cytotoxic and pro-apoptotic activity against breast cancer cell line MCF-7. *Eur. J. Med. Chem.* **2018**, *143*, 1807–1825. [[CrossRef](#)]